DET NORSKE VERITAS

Final Report

Pipeline Segment-Specific External Corrosion Rate Estimation to Improve Reassessment Interval Accuracy (#330)

PHMSA
(DTPH56-08-T-000015)

Report No./DNV Reg No.: ENAUS813KKRA (811 8269 1-7)
December 31, 2009

MANAGING RISK

Pipeline Segment-Specific External Corrosion Rate Estimation to Improve Reassessment Interval Accuracy (#330)	DNV COLUMBUS, INC. Materials & Corrosion Technology Center 5777 Frantz Road Dublin, OH 43017-1386, United States Tel: (614) 761-1214 Fax: (614) 761-1633 http://www.dnv.com http://www.dnvcolumbus.com
For:	
Account Ref.:	

Date of First Issue:	December 31, 2009	Project No.	811 8269 1-7
Report No.:		Organization Unit:	Materials/Corrosion Technology Ctr.
Revision No.:	1	Subject Group:	
Summary:			
USA			

Prepared by:	Katherine M. Krajewski, Ph.D. Senior Engineer	*Signature* Katherine M. Krajewski
Verified by:	Oliver C. Moghissi, Ph.D. Director, Materials & Corrosion Technology Center	*Signature* Oliver C. Moghissi
Approved by:	Oliver C. Moghissi, Ph.D. Director, Materials & Corrosion Technology Center	*Signature* Oliver C. Moghissi

☑	No distribution without permission from the client or responsible organizational unit (however, free distribution for internal use within DNV after 3 years)	**Indexing Terms**	
☐	No distribution without permission from the client or responsible organizational unit	Key Words	
☐	Strictly confidential	Service Area	
☐	Unrestricted distribution	Market Segment	

Rev. No. / Date:	Reason for Issue:	Prepared by:	Approved by:	Verified by

Table of Contents

List of Tables

List of Figures

1.0 BACKGROUND

External corrosion growth estimates are required for determining integrity reassessment intervals. Commonly utilized methods are presently limited because they a) do not adequately reflect local conditions of a specific pipeline segment, b) do not reflect corrosion rate distributions (arising from both the stochastic nature of corrosion and non-uniform soil conditions along a pipeline length), and/or c) do not consider the unsteady rate of corrosion over long periods. Three methods to predict corrosion rate are commonly used, and two additional factors are available for consideration:

1. A representative (or severe) defect is sized and divided by a time period. This can be a depth measurement at a direct examination divided by years since pipeline construction. Similarly, it can be an analysis of consecutive ILI inspections. The first limitation to this approach is the assumption that a defect grew uniformly over the period. Corrosion rates are typically not constant over time either because of corrosion product formation or environmental changes. In addition, initiation time for coating failure and corrosion are not considered. The second limitation to this approach is that corrosion rate distributions are not considered in direct examinations and are difficult to interpret from consecutive ILI runs.
2. Corrosion rates are taken from available literature. NACE RP0205 on ECDA suggests the use of 16 mils per year (mpy) when other data is not available, but this number does not reflect the differences in corrosion rates on specific pipelines in specific environments. The number is overly conservative for most pipelines (i.e., it results in an impractically short interval), and it does not represent pipelines with anomalously high corrosion rates. A significant improvement over using one corrosion rate (or range) for all pipelines is to use corrosion rates based on soil type (e.g., Ricker[1]) including an estimate for maximum corrosion depth given the size of a sample. However, matching the soils by geological properties is not expected to accurately match corrosivity. The use of literature values of corrosion rates is therefore not expected to be generically valid for all pipelines (or the specific pipeline of interest). This is because they cannot be uniformly applied to specific pipelines because the environments differ, and the distribution of corrosion along a pipeline is largely ignored.
3. A third method is to take corrosivity measurements at an excavations site where corrosion was discovered. One way to estimate soil corrosivity is to take samples for laboratory electrochemical measurements. A significant improvement is to utilize linear polarization resistance (LPR) on exposed pipe using the surrounding soil or underneath coating

[1] "Analysis of Pipeline Steel Corrosion Data from NBS (NIST) Studies Conducted Between 1922-1940 and Relevance to Pipeline Management," NISTIR 7415 (2007).

disbondments.[2] These methods are limited because a single measurement of corrosivity does not adequately represent the time to first failure nor does it necessarily lead directly to providing insight into appropriate reassessment intervals.

4. A fourth method[3] (not commonly used) utilizes fundamental corrosion models coupled with monitoring methods. This approach is limited because 1) the models are complex and computationally intensive and rely on difficult to obtain information, 2) the corrosion rate experienced by the pipe is not specific to a local environment, so it might not be any more representative than a literature value, and 3) the distribution of corrosion is not considered.

5. A fifth factor to consider is the distribution of corrosion rates. Failures of pipelines do not occur simultaneously at all locations; they are distributed not only over spatial domains but also temporally. However, the mean time-to-failure for a pipeline is often thought to be a characteristic of design life. If the mean value of data is used for life prediction, it implies that failure of 50% of the locations can be tolerated. Of course, the greatest interest is not when 50% of the failures occur; rather, it is when the first failure occurs. The earliest failures may occur substantially earlier than the mean (or median) value. For example, a pipeline with 10,000 corrosion defects, the first defect to fail occurs at 1/10,000 or 0.0001 probability. The first location to fail is obviously of interest because it results in a leak or rupture. When this first failure occurs relative to the mean depends on the nature of the statistical dispersion of the data. Adopting an existing method to predict time to first failure based on short-term measurements,[4,5] ILI inspection data, DA results, and historical information would address this concern and could be adopted into a standard methodology for prioritizing direct inspection locations.

This project builds upon results of previous research in three areas to develop a new method with application that cannot be achieved by any one area by itself. The three areas are described below:

1. Measuring and predicting corrosion rates have been a topic of corrosion science research for more than 100 years. This includes recent past projects on corrosion in soils.[2,3] This project draws upon previous work to predict the effect of cathodic protection on corrosion rates and considers Ricker's[1] work that illustrated that corrosion rates in soil are not represented by a single value.

[2] "Corrosion Growth Rates for Determining Integrity Verification Reassessment Intervals", CC Technologies Final Project Report R4077 (2005).

[3] "Determining Integrity Reassessment Intervals Through Corrosion Rate Modeling and Monitoring", DOT Contract DTRS56-04-T-0002, Southwest Research Institute.

[4] R. Staehle, 'Predicting the First Failure,' CORROSION/2003 Research Topical Symposium, NACE (2003).

[5] P.M. Aziz, 'Application of the Statistical Theory of Extreme Values to the Analysis of Maximum Pit Depth Data for Aluminum,' Corrosion vol. 12, no. 10, NACE (1956).

2. Methods to use a distribution of corrosion data to predict time to first failure have previously been developed,[4,5] but they have not been applied to corrosion in soils. This project identifies the best method to apply corrosion data distributions to corrosion in soils.
3. Integrity management principles have evolved over the past 5 to 10 years. This project is consistent with these principles so that it can support existing management plans (including compliance with federal regulations).

2.0 OBJECTIVES AND DELIVERABLES

The primary objective of this research was to provide a simple tool to optimize determination of integrity reassessment intervals by more accurately predicting external corrosion rates that are 1) representative of a specific pipeline segment and 2) include distribution of corrosion rates (allowing prediction of time-to-first-failure).

Secondary objectives of this research included 1) putting recently reported NIST data into a context that can be used by pipeline operators and 2) including the ability to allow reduction of predicted corrosion rate based on cathodic protection data.

3.0 TECHNICAL APPROACH

The work scope consisted of six tasks that focused on the development of a method to estimate segment-specific external corrosion rates based upon excavation data collected at a single time point. The work builds upon previous research, incorporating such factors as soil parameters, coating parameters, and level of cathodic protection, while maintaining a consistency with integrity management principles.

The six tasks that comprise this project are:

- Task 1 – Develop Method to Apply Corrosion Rate Distribution
- Task 2 – Develop Method to Apply NIST Corrosion Data
- Task 3 – Develop Method to Reduce Predicted Corrosion Rate from Monitoring Data
- Task 4 – Develop Reassessment Protocol
- Task 5 – Incorporate Protocol in MS Excel Spreadsheet
- Task 6 – Demonstrate Protocol and Refine

The purpose and details of each task are given below.

3.1 Task 1: Develop Method to Apply Corrosion Rate Distribution

Corrosion occurs with a distribution of rates making the use of one value limited in accuracy; see Figure 1. On the average, pipeline corrosion is typically very low. However, few locations of high corrosion rate are the source of an integrity threat. This concept is the basis of Direct Assessment methods where these isolated locations are to be identified and evaluated.

Task 1 included a literature review of corrosion distribution functions with respect to pipelines. Specifically, the review identified recent advances in the understanding of the influence of soil, coating, and cathodic protection factors on external corrosion of buried pipe. Existing methods/models were evaluated to determine which ones were available and held the most promise.

3.2 Task 2: Develop Method to Apply NIST Corrosion data

The NIST corrosion data used for this project was obtained from a report published by Richard Ricker entitled "Analysis of Pipeline Steel Corrosion Data from NBS (NIST) Studies Conducted Between 1922-1940 and Relevance to Pipeline Management." The data was collected from bare steel pipe that was exposed to different soil types across the United States. A total of 47 sites were included in the study. The published data included maximum pit depths and maximum penetration rates at multiple exposure times as well as physical soil characteristic for each site.

Figure 2 is a plot showing the classification of soils based upon clay, sand, and silt composition. Of the 47 sites published by NIST, only 34 of the sites contained soil information. The soils fell within 12 different soil types. Figure 3 contains plots of maximum pit depths vs. exposure time for the 12 soil types identified in the NIST data. As seen in the figure, each soil type contained data for two separate sites, at a minimum.

The NIST data was used to evaluate and verify how applicable the selected corrosion model/method was for predicting corrosion rates. The NIST data was utilized by grouping the data according to soil types (e.g. clay, clay loam, sandy clay loam, etc.). The average data for each soil type was then used in the corrosion model to calculate a predicted maximum pit depth (d_{max}). The predicted maximum pit depth was then compared to the actual maximum pit depths reported in the NIST report.

3.3 Task 3: Develop Method to Reduce Predicted Corrosion Rate from Monitoring Data

Corrosion rates are reduced by cathodic protection. The amount of reduction depends on the level of cathodic polarization (approximately a 10-fold reduction for every 100mV). However, it is not expected that a single level of polarization can be used to reduce corrosion rates uniformly. Rather, it is expected that the level of mitigation can be reduced via a distribution of values.

3.4 Task 4: Develop Reassessment Protocol

Task 4 involved the development of a protocol that includes an approach for predicting external corrosion rates and the time to first failure. The protocol was written to be consistent with an operator's Integrity Management Plan intended for federal regulatory compliance and possible incorporation into an industry standard (e.g., NACE). The protocol includes consideration of mitigation techniques such as coating and cathodic protection.

3.5 Task 5: Incorporate Protocol in MS Excel Spreadsheet

A spreadsheet is still in development so that relevant input data can be entered, and a corrosion rate distribution will result that feeds into a reassessment interval determination. It is expected that a maximum corrosion rate and associated likelihood that this rate will be exceeded will result. The format follows what was developed for 1) Internal Corrosion Direct Assessment (ICDA) for dry gas systems and 2) ICDA for liquid petroleum systems (under PHMSA R&D funding). The tool simplicity will allow rapid dissemination of the developed method.

3.6 Task 6: Demonstrate Protocol and Refine

Task 6 was originally proposed to involve demonstration of the technology at dig sites. Due to delays in development of the model, the field visits involved only the collection of data (e.g. historical pipe information, soil, coating, cathodic protection, corrosion data, and linear polarization measurements). This task involved the cooperation of Panhandle, a natural gas transmission pipeline company.

During the field visit, historical pipe information was collected for the pipe segment associated with each dig site. The information collected included the following:

- Date of installation
- Nominal pipe outer diameter (OD)
- Nominal pipe wall thickness
- Type of cathodic protection (CP) on/off potential data
- Coating type
- Specified minimum yield strength (SMYS)
- Maximum allowable operating pressure (MAOP)

- Pipe Manufacturer

Upon excavation of each site, photographs were taken to document the conditions of the site and the pipe segment. At that time, the depth of cover and condition of any pipe coating was noted. Next, soil samples were collected for analysis. At a minimum, one sample from each of the following locations was collected for analysis: (1) at the pipe surface (interface soil) and (2) away from the pipe surface (native soil) but at a comparable depth to the buried pipe. Samples were packaged and transported to DNV Columbus, Inc. *(DNV Columbus)* for analysis. Analyses performed on the samples tested for the following: (1) the concentration of soluble cations, (2) the concentration of soluble anions, (3) pH, (4) total alkalinity, (5) moisture content, (6) linear polarization resistance, and (7) as-received resistivity.

Next, a direct examination of the pipe was performed. External corrosion present on each pipe segment was visually examined and photographed. The maximum depth, length, and width for each external anomaly identified was measured and documented. During the examination, the actual wall thickness of each pipe segment was measured in areas free of anomalies.

Finally, linear polarization resistance (LPR) measurements were performed on the pipe segment from each dig site to estimate the instantaneous corrosion rates. LPR measurements represent the resistance of the interface to direct current flow and are inversely proportional to the corrosion rate according to the following Stern Geary equation:

$$R_p = \left[\frac{d\varepsilon}{di_{app}}\right]_{\varepsilon \to 0} = \left[\frac{\Delta\varepsilon}{\Delta i_{app}}\right]_{\varepsilon \to 0} = \frac{\beta_a \beta_c}{2.3 \times i_{cor}(\beta_a + \beta_c)} = \frac{B}{i_{cor}} \qquad (1)$$

Where: $\mathbf{i_{cor}}$ = the corrosion rate

$\boldsymbol{\beta_a}$ = the anodic Tafel constant

$\boldsymbol{\beta_c}$ = the cathodic Tafel constant

$\mathbf{R_p}$ (or PR) = the polarization resistance defined as $d\varepsilon/di_{app}$.

B = a proportionality constant, also called "environment constant"

This equation indicates that for small deviations from the free corrosion potential (+/-5 to +/-20 mV), the corrosion rate is inversely proportional to R_p. It also shows that R_p is equal to the slope ($d\varepsilon/di_{app}$) of the linear plot of potential versus current at the free corrosion potential. Thus, polarization resistance measurements can be determined using instrumentation that is able to produce an **E** (potential) **vs i** (current) plot for the range of +/-20 mV relative to the free corrosion potential and that is able to calculate the slope of that curve.

For this project, all LPR measurements were made using a Polarization Resistance Monitor PR4500, manufactured by CC Technologies Services, Inc; see Figure 4. The PR4500 is an instrument specifically designed to measure the polarization resistance of a corroding electrochemical interface, such as a pipe. The PR4500 utilizes a potential control stepping sequence that is flexible and programmable by the operator. Figure 5 is a screenshot showing the setup menu options available for the LPR measurements on the PR4500. At the end of the standard polarization measurement cycle, an AC signal is applied to the working electrode (pipe in this case) for the purpose of measuring the solution resistance, R_s. Finally, a corrosion rate was calculated from i_{cor} value as follows (R_p units in equation (1) are ohm×m^2):

$$CR(mpy) = 1.248 \times \left[\frac{i_{cor} \times M}{n \times F \times D} \right] \qquad (2)$$

Where: $\mathbf{i_{cor}}$ = mA/m^2

D = density, g/cm^3

M = molecular weight, g/mole

F = 96,490 coulomb/eq

n = number of electrons transferred (valence)

Figure 6 is a screenshot showing the representative processed values displayed by the PR4500 at the end of each linear polarization test.

To simulate conditions in the field, a corrosion cell was made on the pipe using a small diameter acrylic tube, interface soil samples, a $Cu/CuSO_4$ electrode (reference electrode), and a graphite ring electrode (counter electrode); see Figure 7. The tube was placed on the bare pipe surface and partially packed with interface soil. The $Cu/CuSO_4$ electrode (reference electrode) and a graphite ring electrode (counter electrode) were then positioned within the cell and then the remainder of the tube was packed with interface soil. Next, electrical leads from the PR 4500 were connected to the pipe (working electrode), a $Cu/CuSO_4$ electrode (reference electrode), and a graphite ring electrode (counter electrode).

The field data for each dig site was later analyzed using the selected corrosion model and the predicted corrosion rates were compared to the actual corrosion rates to gauge consistency.

4.0 RESULTS AND DISCUSSION

4.1 Task 1: Develop Method to Apply Corrosion Rate Distribution

Deterministic and stochastic (statistical) are two methods commonly used to assess corrosion failure life. Although deterministic methods are acceptable for certain applications, they are relatively simplistic and do not consider all the complexities of the corrosion process (i.e. effects of metallurgical and environmental variables). Deterministic methods typically use known corrosion rates, determined either in the field or the laboratory, to predict or estimate corrosion life. Corrosion predictions are thus based upon the assumption that all corrosion defects within the structure grow at a single corrosion rate. Accordingly, this method tends to overestimate the severity level of several defects while underestimating the severity level of a handful of defects. The emphasis of the method on a single defined corrosion rate is thus more applicable to general corrosion rather than localized corrosion. Localized corrosion, however, accounts for more unexpected losses than general corrosion due to difficulties in its detection and prediction. Consequently, identifying a means to predict localized corrosion rates is critical for the assessment of external corrosion and for this study.

Stochastic or statistical methods are more accurate for predications of corrosion life [1] as they tend accommodate and incorporate the natural variation of metallurgical, environmental, and other factors that occur during the corrosion process. The statistical nature of multiple factors associated with localized corrosion was first identified by Evans *et. al.* [2], who introduced the concept of corrosion probability and stressed its importance *vs.* deterministic methods [3]. Thus, in contrast to deterministic methods, stochastic/statistical methods assess corrosion life as a probability of occurrence and are more appropriate for the intent of this work.

Common statistical methods for assessing corrosion rates include normal distributions and extreme value distributions. Normal (Gaussian) distributions typically assess data with regard to two main parameters: the mean (μ) and the standard deviation (σ). Use of these distributions incorporates the mean time-to-failure for a pipeline as the characteristic of design life. While appropriate for some applications, assessing the design life of a pipeline by using the mean time-to-failure does not account for early failures. These failures may occur substantially earlier than the mean (or median) value. Thus, distributions that account for the first location to fail (i.e. via a leak or rupture) are of critical interest. In contrast, extreme value distributions involve the stochastic behavior associated with the maximum and minimum values of random variables.

Therefore, these distributions, which only consider the extreme values extracted from the larger sample, can more accurately model defect extremes. Advantages associated with these distributions include that they are simple, versatile, and focus on high priority data.

A review of the literature identified three types of extreme value distributions including: (1) Type I known as the Gumbel distribution, (2) Type II known as the Frechet distribution, and (3) Type III known as the Weibull distribution. All three distributions can be considered in the generalized cumulative distribution function (CDF) shown in Equation 3 [4].

$$GEV(u,\alpha,k) = \exp\{-[1-k(x-u)/\alpha]^{\frac{1}{k}}\} \quad kx \le \alpha + uk \qquad (3)$$

Where: u = the location parameter, α = the scale parameter, k = shape parameter, and x = pit depth/charge passed.

The shape parameter (k), whose influence is subtler, can play a dominant role in determination of the overall distribution. In fact, it is the shape parameter that indicates which extreme value distribution accurately fits the data. The specific distribution is easily identified by the sign and value of k. Distributions in which the k = 0 correspond to the Gumbel distribution. Accordingly, distributions in which the k < 0 and k > 0 are associated with the Frechet and Weibull distributions, respectively. The probability distribution functions (PDF) corresponding to the Gumbel, Frechet, and Weibull distributions are shown in Equations 4-6.

$$Gumbel\ PDF = F(x) = \exp(-\exp[-\frac{x-u}{\alpha}]) \qquad (4)$$

$$Frechet\ PDF = F(x) = \exp(-x^{-k}) \qquad (5)$$

$$Weibull\ PDF = F(x) = 1-\exp(-(\frac{x-u}{\alpha})^{k}) \qquad (6)$$

The most frequently used extreme value distributions for corrosion rate distributions were found to include the Gumbel and the Weibull type distributions. These two distributions are based upon the largest and smallest values, respectively. A review of these distributions revealed that researchers typically use the Gumbel distribution when predicting maximum pit depths [5, 6] and the Weibull distribution when predicting time-to-first-failure (or weakest link). Consequently, Weibull distributions appear to be the most promising method for this investigation.

A literature review of the approaches used with regard to corrosion rate distributions yielded commonalities in their incorporation of maximum pit depths. Although the statistical nature of corrosion has been known for several years, common application of statistics to routine pipeline inspections has typically not been applied. Thus, the approaches reviewed, while stochastic in nature, varied extensively.

Some of the earliest applications of extreme value methods to assess external corrosion conditions of pipelines were conducted by both Gumbel [7] and Hawn [8]. Both researchers considered the maximum pit depth/size in their respective evaluations.

Since the work of Gumbel and Hawn, researchers have focused on improving the accuracy of corrosion rate predictions by extreme value methods. The approaches have varied from characterization of pitting and growth, incorporation of inspection data, consideration of remaining strength, and incorporation of pipe and soil characterization.

Of the four approaches used to improve the accuracy of extreme value prediction methods, the most extensive research has been in accurately characterizing pitting, pit initiation, and pit growth. Researchers that focused in this area included Worthingham *et. al.*, Fenyvesi *et. al.*, Melchers *et. al.,* Valor *et. al,* and Alfonso *et. al*. The approach and findings of these researchers is presented below.

Worthingham *et. al.* [9] used multiple in-line inspection data from one line to develop the One Run Growth (ORG) method. This method allowed for the prediction of corrosion rates on another line from single inspection data. These investigators not only determined distribution rates for all defects, but also determined the distribution of corrosion rates as a function of depth. While allowing for improved prioritization with respect to their inspection programs, this method only considered the location, size, and depth of the defects. Consideration of the effects of metallurgical and environmental variables was not considered.

Fenyvesi *et. al.* [10] investigated two possible corrosion pit growth models for predicting the development of corrosion pits on an operating pipeline. The two models were identified as the Slowing Pit Model and the Stochastic Pit Growth Model. The Slowing Pit Model was based upon the assumption that pits grow at a characteristic rate. In contrast, the Stochastic Growth Model was based upon the assumption that pits do not grow at a characteristic rate, but rather have variable growth rates. Data for both models were obtained from in-line inspection (ILI) data taken 25 years after construction and were fit to the Gumbel distribution. The results of their investigation revealed that neither model accurately predicted the distribution of deep defects (i.e. extreme tail of defect depth distribution). While the Stochastic Pit Growth Model tended to underestimate the probability of finding deep defects, the Slowing Pit Model tended to provide overestimations. In the end, the inaccuracies of the models were attributed to over simplified assumptions. The results of their investigations highlight the need for (1) more complex corrosion rate distributions and (2) consideration of influencing factors beyond pit depths. Such factors to consider include the effects of pit interactions, pit shape, soil conditions, pipe conditions, or cathodic protection, all of which affect the remaining life of the defect.

Melchers *et. al.* [11] investigated the effects of pitting and exposure time on probability distributions based on maximum pit depths. Their findings identified differences in pitting behavior due to metastable (shallow) pitting and stable (deep) pitting. In addition, they observed that changes in the governing corrosion process affected the fit of maximum pit depth data to the Gumbel distribution for long exposure times. The corrosion processes specifically identified were those driven by oxygen and those driven by bacteria. While initially corrosion may be governed by the rate of oxygen transport to the metal surface, over time corrosion may be controlled by the transport of essential nutrients to bacteria. Whereas the Gumbel distribution did not accurately represent the maximum pit depth data at long exposures, Melchers found that the Fréchet distribution did. Specifically the Fréchet distribution was a better fit for the upper tail of the corrosion distribution when considering bacteria driven corrosion and increased exposure times. These findings indicate that use of the Gumbel distribution, which is still used by many researchers, may not be the best model. Rather, the Fréchet distribution may be more accurate in certain situations.

Valor *et. al.* [12] developed a corrosion distribution model that considered the effects of pit initiation and growth. The investigators realized that the two aspects of pitting could be more accurately depicted by separating them into two stochastic processes. Pit initiation was modeled using exponential and Weibull distributions that accounted for multiple pit initiation events. Using this model, pit initiation time was related to a time to first failure (i.e. passive film breakdown). Pit growth was modeled using a non-homogeneous Markov process. The result was a five parameter model incorporating both the pit initiation and pit growth processes and based upon extreme value statistics. Similar to many other investigators, Valor *et. al.* verified their model using the Gumbel distribution. While adaptable to a variety of material and corrosive environments, the model does not consider the influence of pipe and soil parameters.

Alfonso *et. al.* [13] addressed maximum pit distributions based upon pit densities and spatial distributions common to pipelines. Using magnetic flux leakage (MFL) and ultrasonic in-line inspection (ILI) data, these researchers conducted Monte Carlo simulations to assess the influence of inspection areas (size and number) on the prediction accuracy of homogenous and non-homogeneous pit distributions. Based upon their results, they determined that 1 to 3% of the total pipeline area should be inspected in order to achieve standard deviations on the order of

MFL tools. The most significant finding was that larger inspection areas were necessary as clustering of pitting increased.

Another approach for the improvement of extreme value methods has involved incorporation of inspection data. Specifically, this approach has incorporated data obtained during above ground surveys (corrosion and coating) and pig data. Researchers that have focused on this area include Francis *et. al.* and Pogonec *et. al*. The approach and findings of these researchers is presented below.

Francis *et. al.* [14] developed a probabilistic methodology for estimating corrosion defect depth distributions based upon the ECDA methodology. The investigators compared and updated probabilistic distributions based upon data (corrosion growth rates) from corrosion and coating surveys to data obtained from direct assessments (i.e. excavations). Together this information was used to determine the probability of detection and false indications. Using a repair threshold criterion, the methodology was used to determine the probability that a defect exceeding the repair criteria remained and whether continued excavations were necessary. Some identified improvements to the methodology included incorporation of a probability of failure criterion.

Pognonec et. al. [15] also considered developing a methodology in combination with a reliable software tool to optimize re-inspection intervals. Their methodology was based upon corrosion growth rates determined from pig data. Factors that they considered in their methodology included corrosion growth rates, pipe characteristics, and geometric data for corrosion defects. Using Monte Carlo probabilistic methods, the Cross Entropy method, and threshold values, Pognonec developed a tool to determine the punctual and annual probability of failure associated with each defect as well as per kilometer of pipe. Drawbacks to this approach include the absence of soil property and cathodic protection considerations.

A third approach for improving extreme value methods have addressed pressure and remaining strength calculations. Caleyo et. al [16] used this approach. In their investigations, they considered the probabilistic prediction of remaining strength of pressurized pipelines for active corrosion defects using multiple failure pressure models. The models included the extensively used modified B31G and first-order second moment (FOSM) iterative models as well as the infrequently used Monte Carlo and first-order methods (FOM) models. They found that accurate predictions were dependent on exposure times as well as pit depth. Specifically, more accurate predictions could be determined when deep and shallow pitting was considered as separate entities.

More recently, a few researchers have considered the relationship between pipe and soil properties on extreme value distributions. Although many researchers recognize that pipe and, in particular, soil properties affect corrosion rates, they have not addressed these properties due to the complex nature of the relationship. Researchers that have pursued this approach include Romanoff, Mughabghab et. al., Katano et. al., Race et. al. and Velazquez et. al. The approach and findings of these researchers is presented below.

When considering the influence of soil properties on soil corrosivity, many researchers have utilized Romanoff general power law equation for time evolution of pit depth [17].

$$Y_{max} = \beta t^{\alpha} \qquad (7)$$

Where t = exposure time and β and α = constant regression parameters. Using multivariate regression analysis, researchers used the equation to correlate specific soil and pipe variables to the regression constants β and α. In general, the researchers constrained the correlation such that specific soil and pipe variables were associated with only one of the two constants.

While researchers like Mughabghab *et. al.* [18] considered a limited number of soil parameters (pH and moisture), researchers such as Velázquez *et. al.* have expanded the number of soil properties considered. The additional soil properties considered by Velázquez include ionic content, resistivity, and redox potential. Katano et. al. [19] and Race *et. al.* [20] also considered the effects of soil parameters on pit growth. While Katano considered the influence of such parameters as redox potential, ionic species, and resistivity, Race considered the influence of soil type, cathodic protection, and coating type. Both Katano and Race had some drawbacks in their research, however. The drawbacks associated with Katano's research included the absence of soil texture and coating type considerations on pit growth. Similarly, the main drawback associated with Race's research was the use of subjective score variables to derive the influence of soil and pipe coating on pit growth. Direct relationships between pit growth and the physical soil and pipe parameters were not determined.

Finally, Velázquez *et. al.* and Caleyo *et. al.* [21 - 22] used multivariate regression analysis to determine the influence of various soil and pipe characteristics on external pit growth. Using a modified version of Romanoff's power law model to represent the time dependence of maximum pit depths, the investigators determined the dependence of the model on various soil field measurements; see Equation 8.

$$d_{\max}(t) = k(t - t_0)^{\alpha} \qquad (8)$$

Where t = exposure time, t_0 = pit initiation time, and k and α = constant regression parameters.

Soil measurements considered included pH, resistivity, pipe-to-soil potential, humidity, chloride levels, bicarbonate levels, sulfate levels, soil texture, redox potential, and coating type. From their analysis, they were able to correlate redox potential (rp), pH (ph), resistivity (re), and ionic species content (chloride (cc), sulfate (sc), and bicarbonate (bc)) to regression constant k; see Equation 9. Pipe-to-soil potential (pp), water content (wc), bulk density (bd), and coating type (ct) were similarly correlated to regression constant α; see Equation 10.

$$k = b_0 + b_1\, rp + b_2\, ph + b_3\, re + b_4\, cc + b_5\, bc + b_6\, sc \qquad (9)$$

$$\alpha = a_0 + a_1\, pp + a_2\, wc + a_3\, bd + a_4\, ct \qquad (10)$$

Using these correlations, the researchers developed a generic and three separate soil specific predictive models for the external pit growth of buried pipelines. The three soil models included clay, sandy-clay-loam, and clay-loam soils. Like others, Caleyo *et. al.* reported that the distribution of maximum pit depths best fit a Fréchet distribution for long term exposure periods (>20 years). This was attributed to the long-term stabilization of diffusion-controlled pit growth process. Further, they determined that the Fréchet distribution was also the best fit for different soils. The extensively used Gumbel and Weibull distributions were both found to be acceptable for shorter exposure times. The main drawback of Velázquez and Caleyo's research was that they did not consider the influence of cathodic protection on the pit growth model.

Comparison of the α parameter in the power law equation determined by Ricker, Katano, and Caleyo revealed wide variations. When environmental factors were not separated out such as in the work by Ricker, the α parameter was determined to be 0.35. When the environmental factors were only incorporated into the k parameter in the power law equation such as in the work by Katano, the α parameter was determined to be 0.41. Finally, when environmental and pipeline conditions were modeled into the k and α parameters, the α parameter was determined to be 0.78. The wide range of α values indicates the need for proper modeling of the α and k parameters. A uniform α value, as was used by Ricker, does not seem appropriate due to large fluctuations in α with different soils.

Based upon the literature review, the method most applicable to this investigation was found to be that of Caleyo et. al.

Literature

1. ASTM G16 "Standard Guide for Applying Statistics to Analysis of Corrosion Data."
2. U. R. Evans, R. B. Mears, and P. E. Queneau, *Engineering*,136 (1933), 689.

3. U. R. Evans, *Localized Corrosion*, R. W. Staehle, ed., NACE, Houston, TX, (1974), 144.

4. M. A. Hill and R.S. Lillard, "Methods for Accessing Pitting Damage in Carbon Steel Exposed to Alkaline Chloride Waste Environments." Corrosion, Vol. 62, No. 9 (2006), 802.

5. T. Shibata, "*Evaluation of Corrosion Failure by Extreme Value Statistics,*" ISIJ International, Vol. 31 (1991), No. 2, 115-121.

6. T. Shibata, 1996 W.R. Whitney Award Lecture, *"Statistical and Stochastic Approaches to Localized Corrosion,"* Corrosion, Vol. 52, No. 11 (1996), 813-830.

7. E. J. Gumbel, *"Statistical Theory of Extreme Values and Practical Applications,"* US Department of Commerce Applied Mathematic Series 33 (1954).

8. D. E. Hawn, "Extreme Value Prediction of Maximum Pits on Pipelines," Materials Performance 1977 (March) 29-32.

9. R. G. Worthingham, L.L. Fenyvesi, T.B. Morrison, and G. J. Desjardins. *"Analysis of Corrosion Rates on a Gas Transmission Pipeline,"* NACExpo/Conference 2002 Technical Paper, Denver, Colorado.

10. L. Fenyvesi, H. Lu, and T. R. Jack, *"Prediction of Corrosion Defect Growth on Operating Pipelines,"* Proceedings of IPC 2004, Calgary, Alberta, Canada.

11. R. E. Melchers, *"Extreme Value Statistics and Long-term Marine Pitting Corrosion of Steel,"* Probabilistic Engineering Mechanics, Vol 28 (2008), 482-488.

12. A. Valor, F. Caleyo, L. Alfonso, D. Rivas, and J. M. Hallen. "Stochastic Modeling of Pitting Corrosion: A New Model for Initiation and Growth of Multiple Corrosion Pits," Corrosion Science, Vol. 49 (2007), 559-579.

13. L. Alfonso, F. Caleyo, J. M. Hallen, J. H. Espina-Hernandez, J. J. Escamilla-Davish, *"Application of Extreme Value Statistics to the Prediction of Maximum Pit Depth in Non-Piggable, Buried Pipelines,* "Proceedings of IPC2008, Calgary, Alberta, Canada.

14. A. Francis, M. McCallum, M. T. Van Os, P. van Mastright,*"A New Probabilistic Methodology for Undertaking External Corrosion Direct Assessment,"* Proceedings of IPC 2006, Calgary, Alberta, Canada.

15. G. Pogononec, V. Gaschignard, and P. Notarianni, *"Predictive Assessment of External Corrosion on Transmission Pipelines,"* Proceedings of IPC 2008, Calgary, Alberta, Canada.

16. F. Caleyo, J. L. Gonzalez, and J. M. Hallen, *"A study on the Reliability Assessment Methodology for Pipelines with Active Corrosion Defects,"* International Journal of Pressure Vessels and Piping, Vol. 79 (2002), 77-86.

17. M. Romanoff, *"Underground Corrosion"* NBS Circular 579, National Bureau of Standard, Washington D. C. (1957).

18. S. F. Mughabghab and T. M. Sullivan, "Evaluation of the Pitting Corrosion of Carbon Steels and Other Ferrous Metals in Soil Systems, "Waste Management, Vol 9. (1989), 239-251.

19. Y. Katano, K. Miyata, H. Shimizu, and T. Isogai, "Predictive Model for Pit Growth on Underground Pipes, "I Corrosion, Vol. 59, No. 2 (2003), 155-161.

20. J. M. Race, S. J. Dawson, L. M. Stanley, and S. Kariyawasam, *"Development of predictive Model for Pipeline External Corrosion Rates,"* Journal of Pipeline Engineering, Vol 6. (2007), 15-29.

21. J. C. Velázquez, F. Caleyo, A. Valor, J.M. Hallen, J. H. Espina-Hernandez, A. Lopez-Montenegro, *"Statistical Modeling of Pitting Corrosion in Buried Pipelines Taking into Account Soil Properties,"* Proceedings of IPC 2008, Calgary, Alberta, Canada.

22. F. Caleyo, J. C. Velázquez, J. M. Hallen, J. E. Araujo, E. Perez-Baruch. *"On the Probabilistic Distribution of External Pitting Corrosion Rate in Buried Pipelines."* Proceedings of 7th International Pipeline Conference 2008

4.2 Task 2: Develop Method to Apply NIST Corrosion data

The NIST published data were analyzed using Caleyo's modified power law equation to predict maximum pit depths. As discussed in Section 4.1, Caleyo's model only considered data from the following soil types: clay, clay loam, and sandy clay loam. The NIST data, however, included 12 different soil types; refer to Figure 3. Thus, the available soil specific regression coefficients for the k and α power law parameters did not cover all the NIST soil types. Figure 8 is a soil classification plot showing the soil types where Caleyo and NIST data was available.

Since clay, clay loam, and sandy clay loam regression coefficients were available from Caleyo's work, the 12 NIST soil types were analyzed according to each of the three soil type models to determine their applicability. For each of the three soil types, the k and α parameters from the modified power law were calculated and compared to Caleyo's published values to gauge their consistency; see Equations 9 and 10 in Section 4.1. The regression coefficients published by Caleyo for each of the three soil types as well as a general ("all") soil type were used in the calculations; see Table 1 for values.

Figure 9 contains plots of actual and predicted maximum pit depths vs. exposure time for the 12 soil types identified in the NIST data based upon Caleyo's clay regression coefficients. As seen in the figure, Caleyo's clay model best fits the NIST clay soil data. The model overestimates the maximum pit depth for most of the other soil types.

Figure 10 contains plots of actual and predicted maximum pit depths vs. exposure time for the 12 soil types identified in the NIST data based upon Caleyo's clay loam regression coefficients. As seen in the figure, Caleyo's clay loam model best fits the NIST clay loam soil data. The model, however, also provides a fair prediction of maximum pit depths for other soil types as well.

Figure 11 contains plots of actual and predicted maximum pit depths vs. exposure time for the 12 soil types identified in the NIST data based upon Caleyo's sandy clay loam regression coefficients. As seen in the figure, Caleyo's sandy clay loam model provides a good fit for the NIST sandy clay loam, sand, and sand loam soil types. The model underestimates the maximum pit depths for all the other NIST soil types.

Figure 12 contains plots of actual and predicted maximum pit depths vs. exposure time for the 12 soil types identified in the NIST data based upon Caleyo's "all" soil regression coefficients. As seen in the figure, Caleyo's "all" soil model can be used to estimate maximum pit depths in other Type II soils; refer to Figure 8. For these soils, the "all" model seems to provide better results than the clay loam model.

4.2.1 Comparison of k and α parameters

The NIST data was grouped according to Caleyo's three soil types (clay, clay loam, sandy clay loam) and the k and α parameters were determined and averaged; see Table 2 for NIST site specific data used for this analysis.

Review of the NIST data for clay soils, revealed 5 sites that directly fit the clay soil category and an additional 5 sites were on the border of fitting the category. To determine whether to include the additional 5 sites, plots of the reported maximum pit depths versus exposure time were made for each site and compared to Caleyo's data. Figure 13 and Figure 14 are the plots for the original 5 clay sites and the additional 5 sites, respectively. As seen in the Figures, the data was fairly consistent with Caleyo's data. Thus, all 10 sites were included in the analysis. The sites, identified as Sites 1, 2, 3, 7, 8, 11, 15, 17, 27, and 42 in the published report, were grouped together and the average physical soil parameters were determined. The results of the calculations are shown in Table 3. As seen in the table, the k and α parameters determined from the NIST clay data appears to be consistent with Caleyo's results.

Review of the NIST data for clay loam soils, revealed 2 sites that directly fit the clay loam soil category and an additional 8 sites were on the border of fitting the category. To determine whether to include the additional 8 sites, plots of the reported maximum pit depths versus exposure time were made for each site and compared to Caleyo's data. Figure 15 and Figure 16 are the plots for the original 2 clay loam sites and the additional 8 sites, respectively. As seen in the Figures, the data for the first two sites was fairly consistent with Caleyo's data while the additional 8 sites exhibited slightly more variation from Caleyo's data. All 8 sites, however, were included in the analysis. The sites, identified as Sites 2, 3, 5, 19, 20, 25, 35, and 42 in the published report, were grouped together and the average physical soil parameters were determined. The results of the calculations are shown in Table 3. As seen in the table, the k and α parameters determined from the NIST clay loam data appears to be consistent with Caleyo's results.

Review of the NIST data for sandy clay loam soils, revealed 1 site that directly fit the sandy clay loam soil category and one additional site that was on the border of fitting the category. To determine whether to include the additional site, a plot of the reported maximum pit depths versus exposure time was made for each site and compared to Caleyo's data; see Figure 17. As seen in the figure, the data was fairly consistent with Caleyo's data. Thus, both sites were included in the analysis. The sites, identified as Sites 16 and 36 in the published report, were grouped together and the average physical soil parameters were determined. The results of the calculations are shown in Table 3. As seen in the table, the k and α parameters determined from the NIST clay loam data were slightly higher than the values determined by Caleyo. The discrepancy between the two may be attributed to the limited sample size for the NIST data.

4.2.2 Summary of NIST data fitting

The following summarizes the findings of the NIST data fitting based upon the three soil categories shown in Figure 8 (Type I, Type II, and Type III soils):

4.2.2.1 Type I soils

- The corresponding available models determined by Caleyo should be used to estimate the maximum pit depth.
- If soil/pipeline data is available, the maximum pit depth can be obtained by plugging all the parameter values into the appropriate Caleyo model.
- If any parameter data is missing, a distribution of the missing parameter obtained from Caleyo's paper can be used to estimate the distribution of the maximum pit depth due to unknown parameters.
- If no soil/pipeline data is available, a distribution of maximum pit depths can be obtained using the distributions of all parameters for that soil type.

4.2.2.2 Type II soils

- The 'Sandy clay loam' model determined by Caleyo should be used for 'sand' and 'sandy loam' soils to estimate the maximum pit depth.

- The ‘all’ soil model determined by Caleyo should be used for all the other Type II soils to estimate the maximum pit depth.

4.2.2.3 Type III soils

- The ‘Sandy clay loam’ model determined by Caleyo should be used to estimate the maximum pit depth for ‘loamy sand’ soils
- The ‘all’ soil model determined by Caleyo should be used to estimate the maximum pit depth for ‘silt’ soils.
- Either the ‘sandy clay loam’ or ‘all’ soil model determined by Caleyo should be used to estimate maximum pit depths for ‘sandy clay’ soils.

4.3 Task 3: Develop Method to Reduce Predicted Corrosion Rate from Monitoring Data

The impact of mitigation techniques such as coating and cathodic protection was incorporated through the method developed by Caleyo et. al..

4.4 Task 4: Develop Reassessment Protocol

DNV Columbus established the following protocol to serve as a guideline to pipeline operators when establishing a corrosion growth rate and reassessment interval for the threat of external corrosion. The DNV Columbus protocol is comprised of eight (8) steps which are described below and should be performed at each excavation area; see Figure 18.

4.4.1 Step 1 – Pipeline Segment Information Collection

The following information should be collected for the pipe sections evaluated to determine an external corrosion growth rate.

Pipeline Segment Information Collection			
GPS Coordinates of Excavation Area[6]:	Lat: Long:	Seam Type:	
Date of Installation:		SMYS[7]:	
Pipe Manufacturer:		MAOP[8]:	
Nominal Outside Diameter:		Coating Type:	
Nominal Wall Thickness:		Cathodic Protection System Type:	
Material Grade:		On/Off Potentials:	

4.4.2 Step 2 – Excavation of Area

- Photodocument the excavation area upon arrival from multiple angles. Please note anything unusual about the excavation area.
- Following the excavation of the area, note and photodocument the depth of cover.
- Following the excavation of the area, note and photodocument the condition of the external coating.
- Photodocument soil stratification in the excavation area. (Photograph the side of the ditch)

4.4.3 Step 3 – Soil Sample and Data Collection

- Collect interface (at the pipe) and native (away from the pipe) soil samples for laboratory analysis. The soil samples should be collected as close as practical to the location of the external corrosion. Package the soil sample for shipment in an air-tight container and mark the container with the date and location at which the sample was collected.

[6] The geographic location information will be used for comparison to national soil databases to indicate the expected soil type of the area.
[7] Specified minimum yield strength
[8] Maximum allowable operating pressure

- Laboratory analysis of the soil samples should include, at a minimum, determination of soil pH, resistivity, linear polarization resistance – corrosion rate, chloride content, sulfate content, bicarbonate content, water content, and bulk density.
- Following the removal of the coating, measure and document the pipe-to-soil potentials.
- Measure and document the soil resistivity.

4.4.4 Step 4 – Direct Examination

- Collect linear polarization resistance (LPR) measurements adjacent to the area of the pipeline that contains the external corrosion.
- Measure and document the actual outside diameter of the pipe sections within the excavation area.
- Measure and document the actual wall thickness in areas free of anomalies for the pipe sections within the excavation area.
- Conduct a direct examination of the external corrosion anomalies using non-destructive examination (NDE) techniques. Photodocument the observed external corrosion anomalies.
- Measure and document the maximum depth, length, and width of each external corrosion anomaly. Each external corrosion anomaly should be measured in the field using the interaction criteria specified in each operator's integrity management program. Document the interaction criteria used to assess the external corrosion.

4.4.5 Step 5 – Distribution of Maximum Pit Depths

4.4.5.1 Type I Soils

Caleyo's modified power law model is applicable for clay, clay loam, and sandy clay loam soils (Type I soils; refer to Figure 8). If the results of the soil analysis indicate that the model is applicable, enter the data obtained from Steps 1, 2, and 3 described above into the MS Excel spreadsheet. Using the power law model described below, the Excel spreadsheet will determine a distribution of maximum pit depths for the specific site for which data was entered.

$$\text{Power Law Model} \qquad d_{\max} = k(t - t_0)^{\alpha}$$

If any parameter data is missing, a distribution of the missing parameter obtained from Caleyo's paper can be used to estimate the distribution of the maximum pit depth due to unknown parameters. If no soil/pipeline data is available, a distribution of maximum pit depths can be obtained using the distributions of all parameters for that soil type.

4.4.5.2 Type II soils

If the results of the soil analysis indicate that Caleyo's model is not applicable but that the soil falls into the Type II soil category (see Figure 8) please select the soil model based on the following:

- If the soil falls in the "sand" or "sandy loam" category, select the "Sandy clay loam" model determined by Caleyo shown on the MS Excel Spreadsheet and enter the data obtained from Steps 1, 2, and 3. Using the modified power law model, the Excel spreadsheet will determine a distribution of maximum pit depths for the specific site for which data was entered.
- If the soil falls in any of the other Type II soil categories, select the "all" soil model determined by Caleyo shown on the MS Excel Spreadsheet and enter the data obtained from Steps 1, 2, and 3. Using the modified power law model, the Excel spreadsheet will determine a distribution of maximum pit depths for the specific site for which data was entered.

4.4.5.3 Type III soils

If the results of the soil analysis indicate that Caleyo's model is not applicable but that the soil falls into the Type III soil category (see Figure 8) please select the soil model based on the following:

- If the soil falls in the "loamy sand" category, select the "Sandy clay loam" model determined by Caleyo shown on the MS Excel Spreadsheet and enter the data obtained from Steps 1, 2, and 3. Using the modified power law model, the Excel spreadsheet will determine a distribution of maximum pit depths for the specific site for which data was entered.
- If the soil falls in the "silt" category, select the "All" soil model determined by Caleyo shown on the MS Excel Spreadsheet and enter the data obtained from Steps 1, 2, and 3. Using the modified power law model, the Excel spreadsheet will determine a distribution of maximum pit depths for the specific site for which data was entered.
- If the soil falls in the "sandy clay" category, select either the "Sandy Clay Loam" or the "All" soil model determined by Caleyo shown on the MS Excel Spreadsheet and enter the data obtained from Steps 1, 2, and 3. Using the modified power law model, the Excel spreadsheet will determine a distribution of maximum pit depths for the specific site for which data was entered.

4.4.6 Step 6 – Corrosion Rate Distribution

Once the maximum pit depth distribution has been performed and review, select the option to calculate the corrosion rate distribution on the MS Excel Spreadsheet. A graph of the corrosion rate distribution will be returned by the program.

4.4.7 Step 7 – Compare the calculated corrosion rates

After the corrosion growth rate distribution is calculated, the reassessment interval should be determined using the criteria specified in the operator's integrity management plan, or in industry accepted standards such as NACE[9] SP0502 or API 1160[10], and the corrosion growth rates calculated as a result of this protocol.

4.5 Task 5: Incorporate Protocol in MS Excel Spreadsheet

Task 5 is still in the development phase and will be supplied at a later date.

4.6 Task 6: Demonstrate Protocol and Refine

Task 6 included collection of soil and direct examination data at dig sites on Panhandle's natural gas transmission system. Six sites were identified for examination and replacement during October of 2009 based upon data collected during a recent in-line-inspection. Panhandle prioritized the sites based upon their calculated rupture pressure ratios (RPR). All six sites were from the same 24-inch diameter line and the data indicated that the sites contained external anomalies. Data from three out of the six digs were available and used for this report. The three dig sites used for this report were identified as Dig Site A2, Dig Site C, and Dig Site D by Panhandle. The details regarding each dig site is described below.

4.6.1 Collection of Field Data

4.6.1.1 Dig Site A2

The first dig site, Dig Site A2, was located in a cultivated bean field and had no notable elevation changes. The portion of the pipe that contained the anomaly was reportedly comprised of 24 inch nominal outside diameter (OD) by 0.312 inch nominal wall thickness. The pipe had a specified minimum yield strength (SMYS) of 35,000 psi and was manufactured by SMLS National Tube. The pipe was installed in 1940, was reportedly coated with Bitumastic 50-B, and

[9] ANSI/NACE SP0502-2008, "Standard Practice – Pipeline External Corrosion Direct Assessment Methodology" NACE International, 2008.
[10] API 1160- 2001, "Managing System Integrity for Hazardous Liquid Pipelines," API Publishing Services, 2001.

had an impressed current cathodic protection (CP) system. The maximum allowable operating pressure (MAOP) of the pipe was reportedly 800 psi.

Figure 19 is a schematic showing the location of the target anomaly identified based upon the recent ILI data. According to the ILI data, the anomaly was located at the 6:30 o'clock orientation, measured 9.61 inches long, and had penetrated through 46% of the wall thickness of the pipe.

Upon excavation of the site, soil samples were collected for analysis. Samples were removed from the following locations for analysis: (1) at the pipe surface (interface soil) and (2) away from the pipe surface (native soil) but at a comparable depth to the buried pipe. The samples were double bagged and transported to DNV Columbus for analysis. Analyses performed on the samples tested for the following: (1) the concentration of soluble cations, (2) the concentration of soluble anions, (3) pH, (4) total alkalinity, (5) moisture content, (6) linear polarization resistance, and (7) as-received resistivity. The results of soil testing conducted on the samples are summarized in Table 4. As shown in the table, Dig Site A2 is slightly acidic, had a high moisture content, and a lower resistivity. These factors contributed to a relatively high corrosion rate as evident by the LPR values. The chloride, bicarbonate, sulfate, and sulfide content of the soil are low in comparison to soil from Dig Sites C and D. The results indicate that the soil is consistent with a clay loam or loam; see Figure 20.

An approximate 40-foot pipe section that contained the target anomaly was removed and transported by a third-party contractor to their facilities for further analysis. At the facility, the area containing the target anomaly was sandblasted to enable more accurate measurement of the corrosion on the pipe. Figure 21 is a photograph showing the area of the target anomaly (identified by ILI) after the pipe was sandblasted. As seen in the photograph, the corrosion in the target area consisted of clustered pits. Dimensional measurements (depth, circumferential length, and longitudinal length) were made on the deepest pits identified on the cleaned pipe section. A total of 26 pits were identified and measured. The results of the measurements are listed in Table 5; refer to Figure 22 - Figure 24 for photographs of the pits. In comparison to the ILI data, corrosion in the vicinity of the target anomaly was approximately 20 inches in length (associated with interacting pits A – U, see Figure 22 - Figure 23) with a maximum depth of 0.114 inches, corresponding to a 37% penetration based upon a nominal wall thickness of 0.312 inches. Thus, the actual pit penetration depth was less than that identified using ILI. The deepest pit fell outside of this area, however. The deepest pit, Pit Y, had a maximum depth of 0.144 inches, corresponding to a 46% penetration based upon a nominal wall thickness of 0.312 inches.

Linear polarization measurements were performed on the excavated pipe segment using the PR4500 at the following locations: (1) bare pipe at the target anomaly, (2) bare pipe adjacent to the target anomaly, and (3) bare pipe away from the target anomaly. The calculated corrosion rates at the target anomaly ranged from 0.07 mpy to 12.5 mpy. The calculated corrosion rates adjacent to the target anomaly ranged from 0.02 mpy to 2.1 mpy. The calculated corrosion rates away from the target anomaly ranged from 0 mpy to 0.2 mpy.

4.6.1.2 Dig Site C

The second dig site, Dig Site C, was located on a steep hillside with notable elevation changes. The portion of the pipe that contained the anomaly was reportedly comprised of 24 inch nominal outside diameter (OD) by 0.312 inch nominal wall thickness. The pipe had a specified minimum yield strength (SMYS) of 35,000 psi and was manufactured by SMLS National Tube. The pipe was installed in 1940, was reportedly coated with Bitumastic 50-B, and had an impressed current cathodic protection (CP) system. The maximum allowable operating pressure (MAOP) of the pipe was reportedly 800 psi.

Figure 25 is a schematic showing the location of the target anomaly identified based upon the recent ILI data. According to the ILI data, the anomaly was located at the 6:00 o'clock orientation, measured 6.27 inches long, and had penetrated through 50% of the wall thickness of the pipe.

Upon excavation of the site, soil samples were collected for analysis. Samples were removed from the following locations for analysis: (1) at the pipe surface (interface soil) and (2) away from the pipe surface (native soil) but at a comparable depth to the buried pipe. The samples were double bagged and transported to DNV Columbus for analysis. Analyses performed on the samples tested for the following: (1) the concentration of soluble cations, (2) the concentration of soluble anions, (3) pH, (4) total alkalinity, (5) moisture content, (6) linear polarization resistance, and (7) as-received resistivity. The results of soil testing conducted on the samples are summarized in Table 4. As shown in the table, Dig Site C is slightly alkaline, had a high resistivity, and a low water content. These factors contributed to a relatively low corrosion rate as is evident by the LPR values. The chloride, bicarbonate, sulfate, and sulfide contents of the soil are high in comparison to soil from Site A2. The actual corrosion rates may be high due to high sulfide contents that were not considered in the Caleyo model. The results indicate that the soil is consistent with silt loam to loam; see Figure 20.

An approximate 52-foot pipe section that contained the target anomaly was removed and transported by a third-party contractor to their facilities for further analysis. At the facility, the area containing the target anomaly was sandblasted to enable more accurate measurement of the corrosion on the pipe. Figure 26 is a photograph showing the area of the target anomaly (identified by ILI) after the pipe was sandblasted. As seen in the photograph, the corrosion in the target area consisted of a mix of general corrosion and pits. Dimensional measurements (depth, circumferential length, and longitudinal length) were made on the deepest pits identified on the cleaned pipe section. The results of the measurements are listed in Table 6. In comparison to the ILI data, corrosion in the vicinity of the anomaly was approximately 8.5 inches in length with a maximum depth of 0.205 inches, corresponding to a 66% penetration based upon a nominal wall thickness of 0.312 inches. Thus, the actual pit penetration depth was greater than that identified using ILI.

In addition to the target anomaly, several secondary anomalies were identified by ILI. These anomalies were located on the pipe section after removal and were identified as Secondary Anomalies A – E; see Figure 27 - Figure 30. Dimensional measurements (depth, circumferential length, and longitudinal length) were performed on the identified anomalies and the results are listed in Table 6.

Linear polarization measurements were performed on the excavated pipe segment using the PR4500 at the following locations: (1) bare pipe at the target anomaly and (2) bare pipe away from the target anomaly. The calculated corrosion rates at the target anomaly ranged from 0.02 mpy to 2.1 mpy. The calculated corrosion rates away from the target anomaly ranged from 0.8 mpy to 4.0 mpy.

4.6.1.3 Dig Site D

The third dig site, Dig Site D, was located on a steep hillside with a ravine just south of the right of way (ROW). The site was downstream (D/S) from a lake and had notable elevation changes. The site was also adjacent to a rectifier and anode bed. The portion of the pipe that contained the anomaly was reportedly comprised of 24 inch nominal outside diameter (OD) by 0.281 inch nominal wall thickness. The pipe had a specified minimum yield strength (SMYS) of 42,000 psi and was manufactured by SMLS National Tube. The pipe was installed in 1939, was reportedly coated with Bitumastic 50-B, and had an impressed current cathodic protection (CP) system. The maximum allowable operating pressure (MAOP) of the pipe was reportedly 800 psi.

Figure 31 is a schematic showing the location of the target anomaly identified based upon the recent ILI data. According to the ILI data, the anomaly was located at the 4:30 o'clock orientation, measured 7.54 inches long, and had penetrated through 48% of the wall thickness of the pipe.

Upon excavation of the site, soil samples were collected for analysis. Samples were removed from the following locations for analysis: (1) at the pipe surface (interface soil) and (2) away from the pipe surface (native soil) but at a comparable depth to the buried pipe. The samples were double bagged and transported to DNV Columbus for analysis. Analyses performed on the samples tested for the following: (1) the concentration of soluble cations, (2) the concentration of soluble anions, (3) pH, (4) total alkalinity, (5) moisture content, (6) linear polarization resistance, and (7) as-received resistivity. The results of soil testing conducted on the samples are summarized in Table 4. As shown in the table, Dig Site D is slightly alkaline, had a high resistivity, and a low water content. These factors contributed to a relatively low corrosion rate as is evident by the LPR values. The bicarbonate and sulfate levels are higher in comparison to Dig Site A2. The low sulfide content may indicate a low real corrosion rate. The results indicate that the soil is consistent with silt loam to loam; see Figure 20.

An approximate 41-foot pipe section that contained the target anomaly was removed and transported by a third-party contractor to their facilities for further analysis. At the facility, the area containing the target anomaly was sandblasted to enable more accurate measurement of the corrosion on the pipe. Figure 32 is a photograph showing the area of the target anomaly (identified by ILI) after the pipe was sandblasted. As seen in the photograph, the corrosion in the target area was consistent with general corrosion. Dimensional measurements (depth, circumferential length, and longitudinal length) were performed on the cleaned pipe section. In comparison to the ILI data, corrosion in the vicinity of the anomaly was approximately 10 inches in length with a maximum depth of 0.104 inches, corresponding to a 37% penetration based upon a nominal wall thickness of 0.281 inches. Thus, the actual pit penetration depth was less than that identified using ILI.

Linear polarization measurements were performed on the excavated pipe segment using the PR4500 at the following locations: (1) bare pipe at the sandblasted target anomaly and (2) bare pipe away from the target anomaly. The calculated corrosion rates at the target anomaly ranged from 0 mpy to 6.1 mpy. The calculated corrosion rates away from the target anomaly ranged from 0 mpy to 0.2 mpy.

4.6.1.4 Dig Site Result Summary

Table 7 summarizes the findings for each dig site analyzed. The first column identifies the soil type for each site. The second column lists the maximum pit depth measured for each dig site. The third column lists the calculated pitting rate equivalent (PRE) values that were determined from the maximum pit depth measurements using the equation below:

$$\text{Pitting Rate Equivalent}\,(\text{mpy}) = \frac{\text{Max pit depth}\,(\text{microns}) * 0.03937\left(\dfrac{\text{mils}}{\text{micron}}\right) * 365\left(\dfrac{\text{days}}{\text{year}}\right)}{\text{exposure period}\,(\text{days})} \qquad (11)$$

As shown in the table, Dig Site C had the highest PRE followed by Sites A2 and D.

4.6.2 Model Fitting of Field Data Using Caleyo's Modified Power Law

The soil data collected from each dig site was analyzed using the modified power law developed by Caleyo et. al. to gauge the consistency of predicted corrosion rates with the actual field corrosion rates. Regression coefficients published by Caleyo et. al. were used to fit the field data.

While the identified soil type for Dig Site A2 fell within the soil types used in Caleyo's models, the identified soil type for Dig Sites C and D did not fall within Caleyo's soil types. Thus, Dig Sites C and D were fitted to all four of Caleyo's models to gauge their applicability. Details regarding the model fitting for all three dig sites are listed below.

4.6.2.1 Dig Site A2

Table 8 and Table 9 summarize the results from fitting the Dig Site A2 soil parameters into the Caleyo modified power law model. Table 8 represents the results when a coal tar coating protection is assumed, while Table 9 represents the results when the coating is assumed to be broken. The regression parameters listed in Table 1 along with the soil data listed in Table 4 were used for the calculations. To verify the soil type identified for Dig Site A2 as well as to determine the consequences of using the wrong soil type model, the data was analyzed using the regression parameters for all three soil conditions (i.e. clay, clay loam, and sandy clay loam). The results were further separated out by their proximity to the pipe (i.e. native or interface soil).

As seen in Table 8, when a coal tar coating was assumed, the clay loam model yielded the closest results (0.81 -1.21 mpy) to the PRE calculated for Dig Site A2 (2.09 mpy, see Table 7). Closer examination of the data revealed that the results associated with the interface soil provided a better predication than that of the native soil. The predicted corrosion rate was still less than the actual corrosion rates. In reviewing the results, the condition of the coating was identified as a parameter that may have been inaccurately assumed. In the field, areas of the coating were missing. Thus, a second analysis of the data was performed assuming a broken coating.

As seen in Table 9, the results again indicate that the clay loam model using the interface soil is the best model for the site. Closer review of the data revealed that the second analysis more accurately predicted the corrosion rate (2.34 mpy) in comparison to the actual corrosion rate (2.09 mpy).

4.6.2.2 Dig Site C and D

Figure 33 through Figure 36 contains plots of maximum pit depth vs. exposure time for all three dig sites when fitted to Caleyo's "Clay," "Sandy Clay Loam," "Clay Loam," and "All" soil models, respectively. The plots were calculated using the regression parameters listed in Table 1 along with the dig site soil data listed in Table 4.

As seen in all four figures, the pipe-to-soil (pp) is an important parameter when predicting maximum pit depths; observe the difference in plots for the upper bound pp values (dotted lines) vs. the mean pp values (dashed lines).

Figure 33 shows the predicted maximum pit depths for all three dig sites when Caleyo's "Clay" model is used. As seen in Figure 33, this model overestimates the maximum pit depth for Site A2.

Figure 34 shows the predicted maximum pit depths for all three dig sites when Caleyo's "Sandy Clay Loam" model is used. As seen in Figure 34, this model underestimates the maximum pit depths for all three dig sites.

Figure 35 shows the predicted maximum pit depths for all three dig sites when Caleyo's "Clay Loam" model is used. As seen in Figure 35, this model provided a good estimate of the maximum pit depth for Dig Site A2, but underestimates the maximum pit depths for Dig Sites C and D.

Figure 36 shows the predicted maximum pit depths for all three dig sites when Caleyo's "All" soil model is used. As seen in Figure 36, this model provided a good estimate of the maximum pit depth for Dig Site A2 and C, but still underestimates the maximum pit depths for Dig Sites C.

4.6.3 Maximum Pit Depth Distribution Fitting for Site A2

A maximum pit depth distribution was calculated for Dig Site A2 using Monte Carlo simulations for each of the modified power law parameters identified by Caleyo in Equations 9 and 10; see Figure 37. Figure 38 contains the resulting probability distribution function of maximum pit depths at 69 years of exposure for Dig Site A2. As seen in the plot, the estimated maximum pit depth at the current exposure time (69 years) is 3.72 mm which is close to actual measured pit depths. In addition, the figure shows the cumulative distribution function which can be used to determine the estimated maximum pit depth in future years.

5.0 SUMMARY

The following is a summary of the key findings:

- With current available corrosion models, one simple equation will not reliably predict corrosion rates in all soil types.
- The method for predicting corrosion rates developed by Caleyo et. al. which is based upon soil parameters is promising for clay, clay loam, and sandy clay loam soils. Their current model, however, does not seem to accurately predict corrosion rates in soils that fall outside of the three defined categories.
- The NIST mean clay, clay loam, and sandy clay loam data follow the general trends predicted by the model developed by Caleyo.
- The location of the soil used for analyses is critical for accurate corrosion rate predictions. Interface soil date yields better predictions than native soil data.
- Determination of the pipe-to-soil potentials is critical for accurate corrosion rate predictions.

6.0 ACKNOWLEDGEMENTS

The researchers would like to acknowledge Yumei Zhai for her significant contributions to the data analyses as well as Narasi Sridhar.

Table 1. Regression coefficients for the maximum pit depth model[11].

Parameter	Soil Type			
	Clay	**Clay Loam**	**Sandy Clay Loam**	**All three soil types**
k_o	5.51 E-01	9.84E-01	5.99E-01	6.08E-01
a_o	8.85E-01	2.82E-01	9.65E-01	8.96E-01
t_o (years)	3.05	3.06	2.57	2.88
k_1 (redox potential, rp)	-8.98E-05	-1.06E-04	-1.82E-04	-1.80E-04
k_2 (pH, ph)	-5.90E-02	-1.15E-01	-6.42E-02	-6.54E-02
k_3 (resistivity, re)	-2.15E-04	-2.99E-04	-2.12E-04	-2.60E-04
k_4 (chloride, cc)	8.38E-04	1.80E-03	8.62E-04	8.74E-04
k_5 (bicarbonate, bc)	-1.28E-03	-4.88E-04	-6.78E-04	-6.39E-04
k_6 (sulfate, sc)	-5.33E-05	-2.09E-04	-1.13E-04	-1.22E-04
a_1 (pipe/soil potential, pp)	4.93E-01	4.61E-01	5.12E-01	5.19E-01
a_2 (water content, wc)	3.72E-03	1.69E-02	4.50E-03	4.65E-03
a_3 (bulk density, bd)	-1.01E-01	-9.87E-02	-1.58E-01	-9.90E-02
a_4 (coating type, ct)	4.67E-01	5.67E-01	4.34E-01	4.31E-01

11 J.C. Velazquez, F. Caleyo, A. Valor, J.M. Hallen, Predictive model for pitting corrosion in buried oil and gas pipelines, Corrosion 65 (2009) 332–342.

Table 2. Chemical and physical properties of clay, clay loam, and sandy clay loam sites reported by NIST[12] .

Site No.	type 2	redox potential	pH	Resistivity, ohm-m	Chloride ppm	Bicarbonate ppm	Sulfate ppm	Pipe to soil potential	bulk density (g/dm3)	coating type
27	clay	0	6.6	5.7	28.4	1.22E+03	1.44E+03	0.00	2.01	1
15	clay	0	7.5	4.9	46.15	1.22E+03	7.01E+02	0.00	2.08	1
8	clay	0	7.6	3.5	3.55	4.33E+02	4.22E+03	0.00	1.56	1
7	clay	0	4.4	21.2	0	0	0	0.00	2.02	1
11	clay	0	5.3	110	0	0	0	0.00	1.49	1
1	clay	0	7	12.2	31.95	5.49E+01	7.97E+02	0.00	0	1
17	clay	0	4.5	59.8	0	0	0	0.00	1.72	1
3	clay	0	5.2	300	0	0	0	0.00	1.6	1
42	clay	0	4.7	137	0	0	0	0.00	1.79	1
2	clay	0	7.3	6.8	14.2	7.32E+02	1.73E+02	0.00	1.95	1
20	*clay loam*	0	7.5	28.7	0	3.11E+02	144	0.00	1.9	1
25	clay loam	0	7.2	17.8	10.65	6.10E+02	9.60E+01	0.00	1.95	1
5	clay loam	0	7	13.5	10.65	4.21E+02	2.40E+02	0.00	2	1
19	clay loam	0	4.6	19.7	10.65	9.76E+01	4.42E+02	0.00	1.76	1
35	clay loam	0	7.3	20.6	21.3	6.71E+02	3.36E+02	0.00	1.89	1
16	sandy clay loam	0	4.4	82.9	0	0	0	0.00	1.65	1
36	sandy clay loam	0	4.5	112	0	0	0	0.00	1.62	1

[12] "Analysis of Pipeline Steel Corrosion Data from NBS (NIST) Studies Conducted Between 1922-1940 and Relevance to Pipeline Management," NISTIR 7415 (2007).

Table 3. Calculated parameters for NIST data using Caleyo modified power law method.

	Caleyo Data			**NIST Data**		
	Clay	**Clay Loam**	**Sandy Clay Loam**	**Clay**	**Clay Loam**	**Sandy Clay Loam**
k	0.18	0.16	0.14	0.16	0.14	0.26
α	0.83	0.79	0.73	0.86	0.79	0.82
Sites	110 sites	61 sites	79 sites	10 sites	8 sites	2 sites

Table 4. Chemical and physical properties of soil samples removed from Dig Sites A2, C, and D.

FIELD ID	Soluble cations mg/kg		SOLUBLE ANIONS, mg/kg							pH soil	Total alkalinity mg CaCO3/kg	Moisture Content %	LPR mpy	As-Received Resistivity Ohm-cm
	Ca^{2+}	Mg^{2+}	NO_2^-	NO_3^-	Cl^-	SO_4^-	S^{2-}	CO_3^{2-}	HCO_3^-					
Site A2 native soil	16.1	16.2	<1.0	<3.0	6.7	<13.56	57	56.1	114.0	6.5	93.5	25.10	2.678	1300
Site A2 interface soil	23.0	8.7	0.062	6.198	5.7	<14.60	<23	60.4	122.8	6.61	100.6	30.43	1.617	1700
Site C native soil	89.5	16.7	0.048	6.432	1.7	39.6	<23	178.7	363.4	8.1	297.9	12.71	2.0456	2700
Site C interface soil	98.8	19.0	0.032	<3.0	7.2	39.27	169	165.9	337.3	8.09	276.5	16.81	1.277	3500
Site C interface soil 12:00	104.7	17.7	0.048	<3.0	4.9	53.89	77	167.7	341.1	7.55	279.6	17.73	1.709	2800
Site C interface soil 9:00	320.9	85.5	0.032	8.491	67.9	784.06	<24	138.3	281.2	7.53	230.5	17.58	2.074	1200
Site D Native soil north end	197.1	25.6	0.032	6.408	3.5	226.82	44	196.7	399.9	8.0	327.8	14.58	1.688	2000
Site D Native soil south end	146.7	19.1	0.047	<3.0	10.5	72.60	62	219.6	446.6	7.99	366	23.51	0.528	5000
Site D interface soil	92.4	25.8	<1.0	<3.0	1.9	<9.76	<24	187.0	380.1	8.12	311.6	19.76	1.391	2000
Site D interface soil at anomaly	33.2	16.8	0.062	<3.0	2.8	9.60	<24	107.6	218.7	7.5	179.3	27.49	0.891	2500

Table 5. Dimensional measurements for Pits A - Z from Dig Site A2. Refer to Figure 22-Figure 24 for locations.

Pit ID	Depth (in inches)	Wall Loss Percentage of Nominal Wall Thickness * (%)	Longitudinal Length (in inches)	Circumferential Length (in inches)
A	0.061	20	0.88	1.00
B	0.048	15	0.25	0.19
C	0.076	24	2.06	1.06
D	0.077	25	1.50	0.75
E	0.092	29	0.50	0.44
F	0.091	29	0.44	0.38
G	0.073	23	0.19	0.31
H	0.060	19	0.19	0.31
I	0.049	16	0.31	0.31
J	0.073	23	0.31	0.50
K	0.067	21	0.44	0.31
L	0.046	15	0.44	0.50
M	0.058	19	0.50	0.63
N	0.073	23	0.44	0.31
O	0.112	36	1.38	1.00
P	0.092	29	1.38	1.19
Q	0.114	37	2.13	1.50
R	0.081	26	0.25	0.25
S	0.081	26	0.75	0.38
T	0.063	20	1.06	0.63
U	0.102	33	0.25	0.31
V	0.081	26	1.50	0.75
W	0.113	36	0.63	0.44
X	0.090	29	1.88	0.44
Y	0.144	46	1.13	0.56
Z	0.075	24	0.25	0.31

* Based upon nominal wall thickness: 0.312-inches

Table 6. Dimensional measurements for the target anomaly and secondary anomalies (Pits A – E) from Dig Site C. Refer to Figure 26 - Figure 30 for locations.

Pit ID	Depth (in inches)	Wall Loss Percentage of Nominal Wall Thickness * (%)	Longitudinal Length (in inches)	Circumferential Length (in inches)
Target Anomaly	0.205	66	8.5	10.25
A	0.190	61	1.5	1.38
B	0.183	59	0.88	1.00
C	0.207	66	1.06	1.00
D	0.167	54	0.75	0.69
E	0.138	44	0.75	0.63

* Based upon nominal wall thickness: 0.312-inches

Table 7. Field measured maximum pit depths and calculated pitting rate equivalents for Dig Sites A2, C, and D.

	Maximum Pit Depth (in)	Pitting Rate Equivalent[13] (mpy)
Site A2	0.144	2.09
Site C	0.207	3.00
Site D	0.104	1.49

[13] $\text{Pitting Rate Equivalent}\left(\text{mpy}\right)=\dfrac{\text{Max pit depth}\left(\text{microns}\right)*0.03937\left(\dfrac{\text{mils}}{\text{micron}}\right)*365\left(\dfrac{\text{days}}{\text{year}}\right)}{\text{exposure period}\left(\text{days}\right)}$

Table 8. Model fitting results for Site A2 assuming a coal tar coating (ct = 0.7).

	Site A2						**Caleyo Results**		
	Clay		**Clay Loam**		**Sand Clay Loam**				
	Native	**Interface**	**Native**	**Interface**	**Native**	**Interface**	**Clay**	**Clay Loam**	**Sandy Clay Loam**
k	0.02	0.00	0.18	0.16	0.10	0.09	0.18	0.16	0.14
alpha	0.76	0.78	0.60	0.69	0.59	0.59	0.83	0.79	0.73
dmax (mm)	0.56	0.10	2.27	2.95	1.21	1.05	5.74	4.52	3.13
dmax (in)	0.022	0.004	0.089	0.116	0.048	0.041	0.226	0.178	0.123
corrosion rate (mm per yr)	0.01	0.00	0.02	0.03	0.01	0.01	0.07	0.05	0.03
corrosion rate (mil per yr)	0.25	0.05	0.81	1.21	0.42	0.37	2.84	2.14	1.36

Table 9. Model fitting results for Site A2 assuming a broken coating (ct = 0.9).

	Site A2						**Calyeo Results**		
	Clay		**Clay Loam**		**Sand Clay Loam**				
	Native	**Interface**	**Native**	**Interface**	**Native**	**Interface**	**Clay**	**Clay Loam**	**Sandy Clay Loam**
k	0.02	0.00	0.18	0.16	0.10	0.09	0.18	0.16	0.14
alpha	0.86	0.88	0.72	0.81	0.68	0.68	0.83	0.79	0.73
dmax (mm)	0.85	0.16	3.73	4.85	1.78	1.54	5.74	4.52	3.13
dmax (in)	0.033	0.006	0.147	0.191	0.070	0.061	0.226	0.178	0.123
corrosion rate (mm per yr)	0.01	0.00	0.04	0.06	0.02	0.02	0.07	0.05	0.03
corrosion rate (mil per yr)	0.43	0.08	1.60	2.34	0.72	0.62	2.84	2.14	1.36

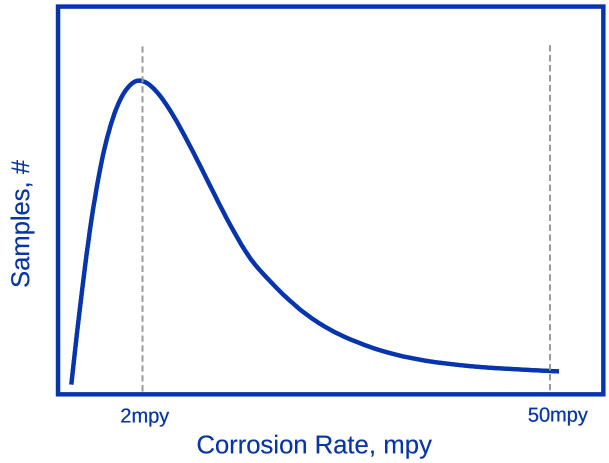

Figure 1. Simple corrosion distribution plot

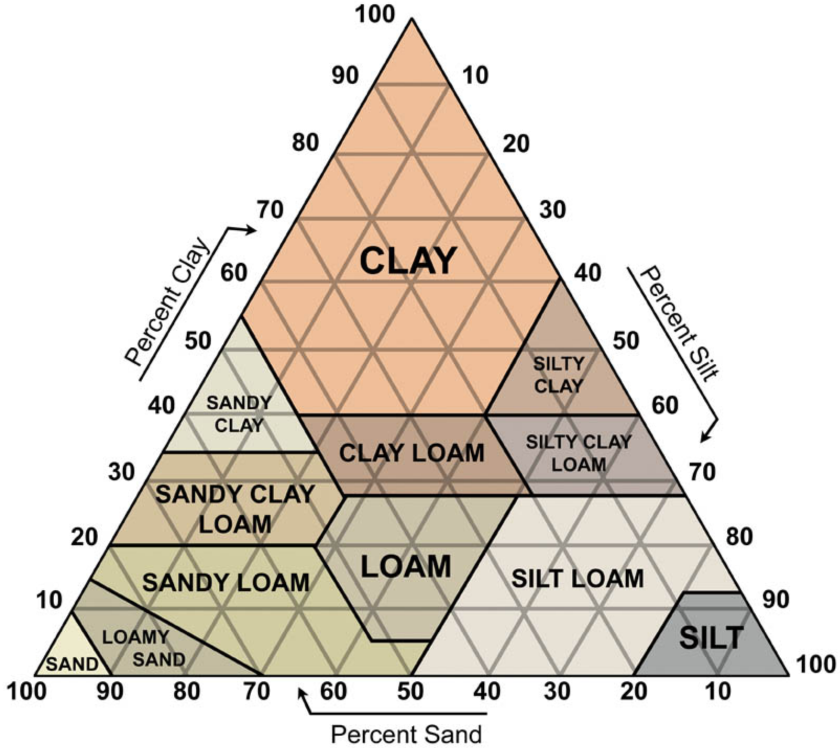

Figure 2. Plot showing soil classifications[14]

[14] http://www.soilsensor.com/images/soiltriangle_large.jpg

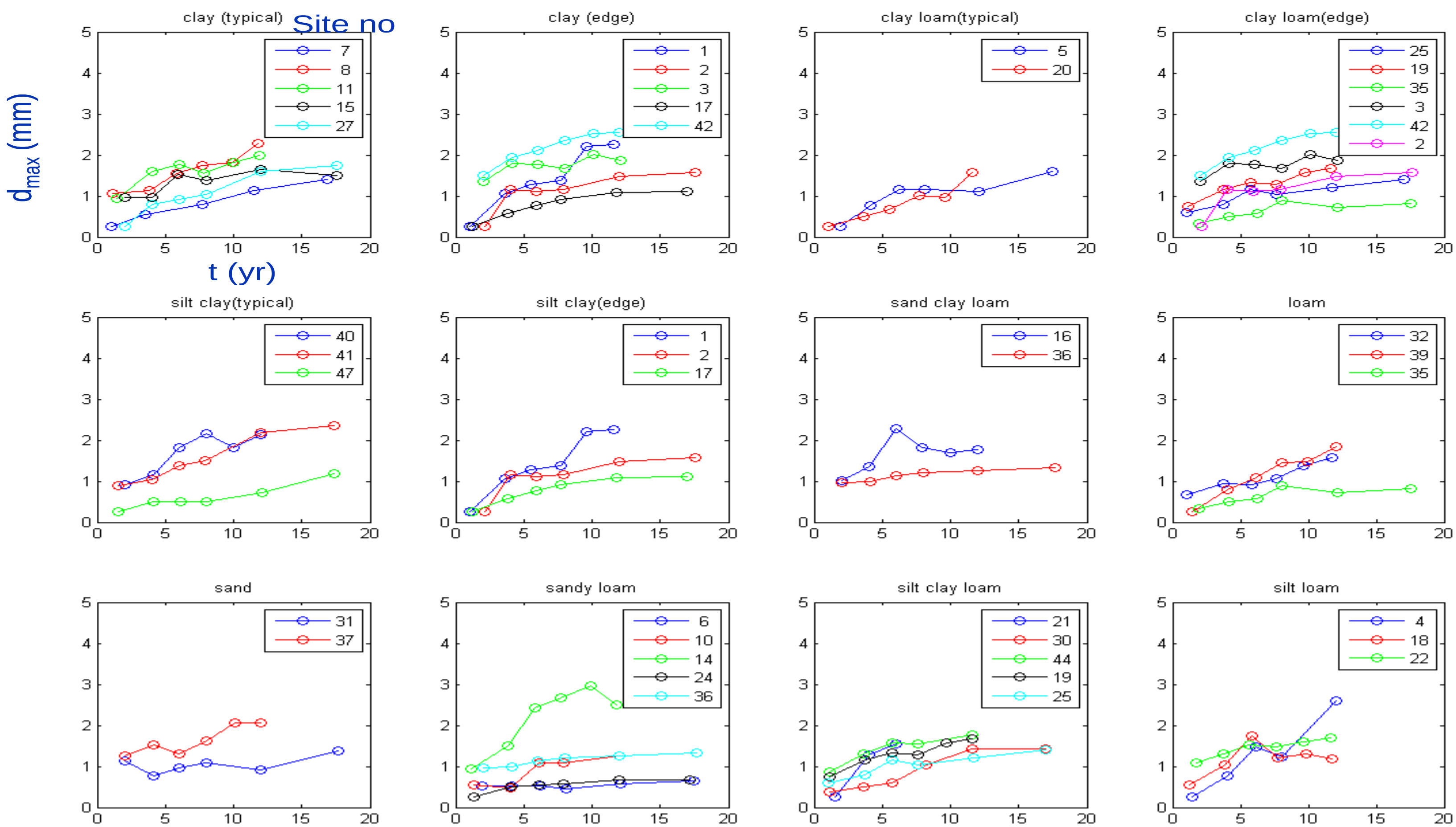

Figure 3. Plots of maximum pit depths (y-axis) vs. exposure time (x-axis) by soil type for the NIST data.

Figure 4. Photograph showing PR4500 data acquisition system and monitor.

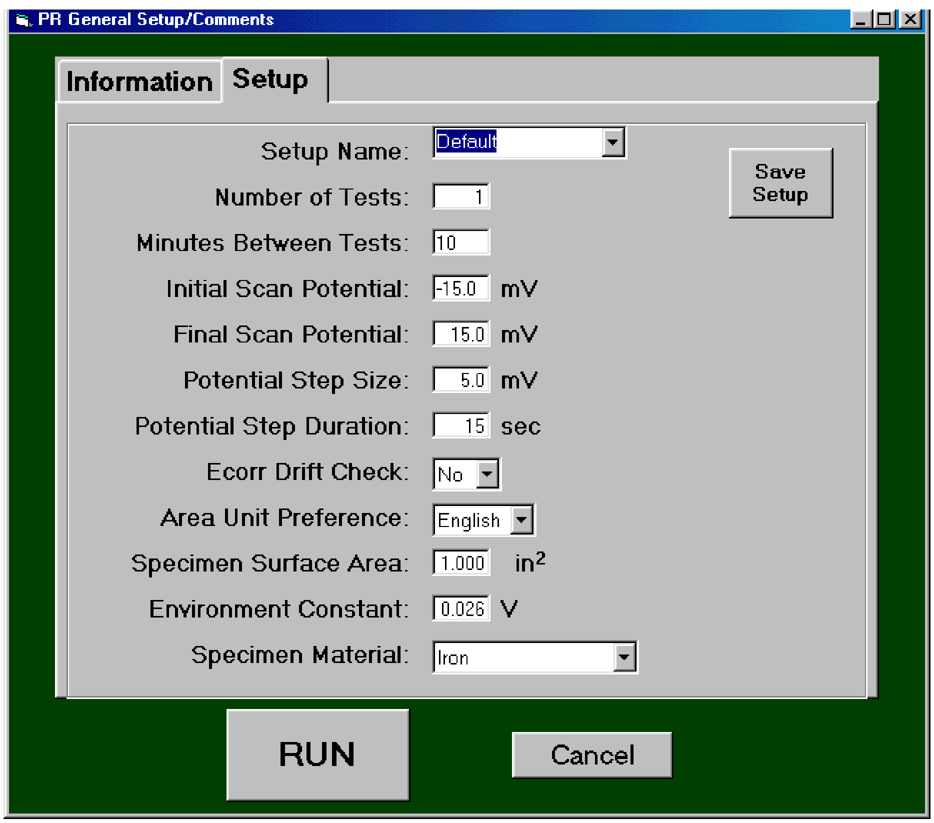

Figure 5. Screenshot showing the setup menu options available for the linear polarization tests.

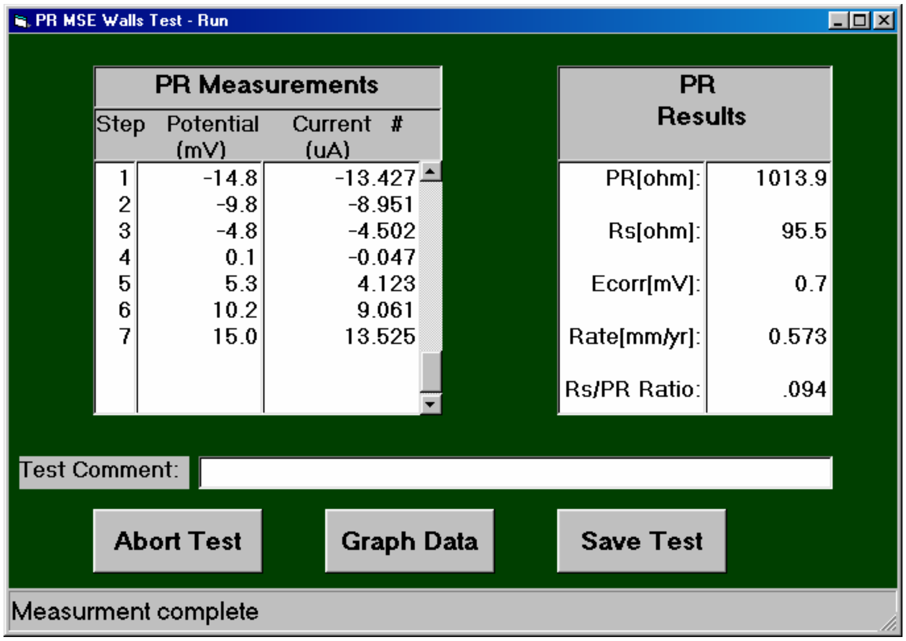

Figure 6. Screenshot showing representative processed values displayed by the PR 4500 at the end of a linear polarization test.

Figure 7. Photograph showing linear polarization cell setup.

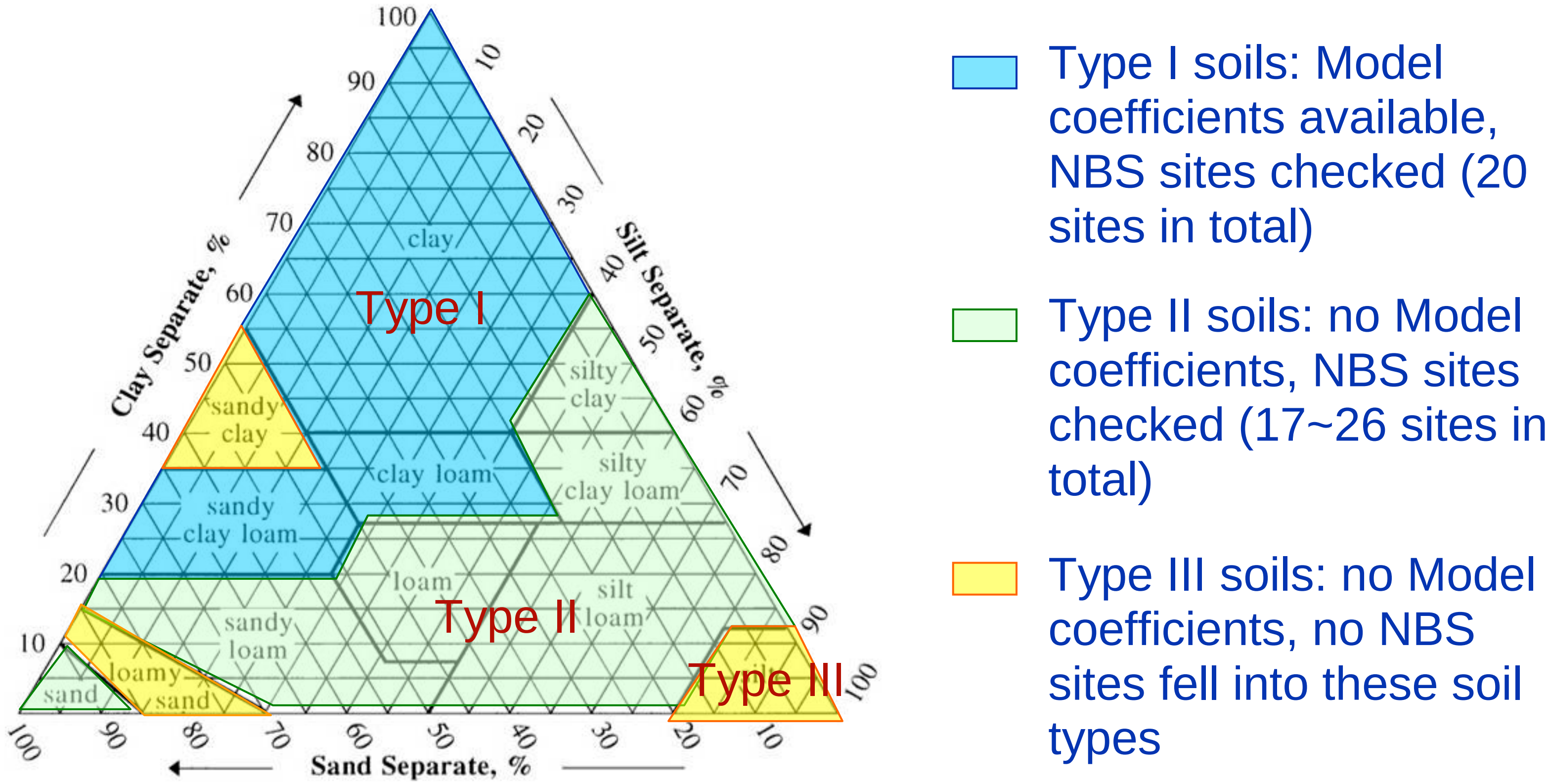

Figure 8. Soil classification plot showing the soil types where Caleyo and/or NIST data are available.

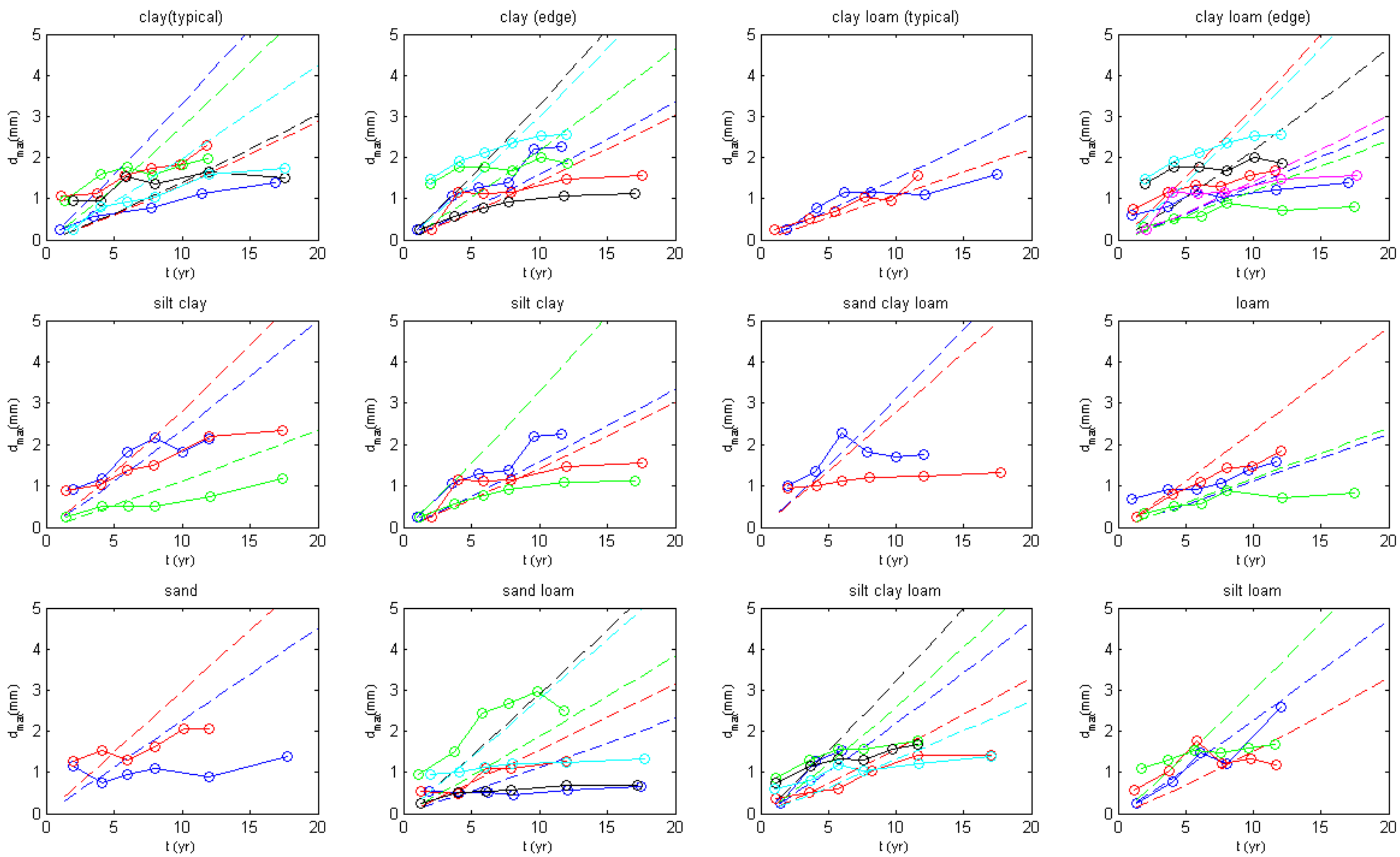

Figure 9. Plots of actual and predicted maximum pit depths vs. exposure time determined from the regression coefficients for clay as determined by Caleyo.

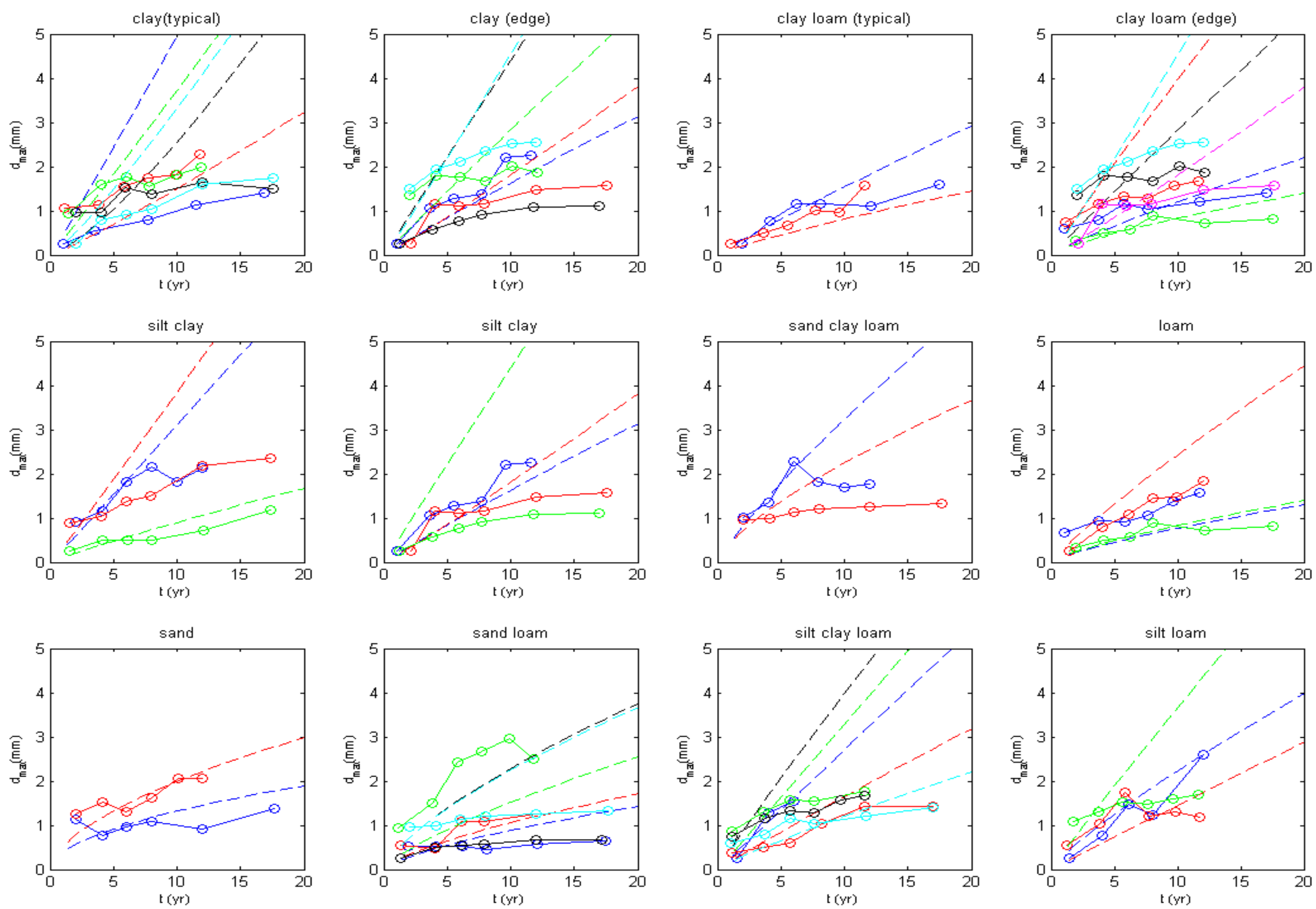

Figure 10. Plots of actual and predicted maximum pit depths vs. exposure time determined from the regression coefficients for clay loam as determined by Caleyo.

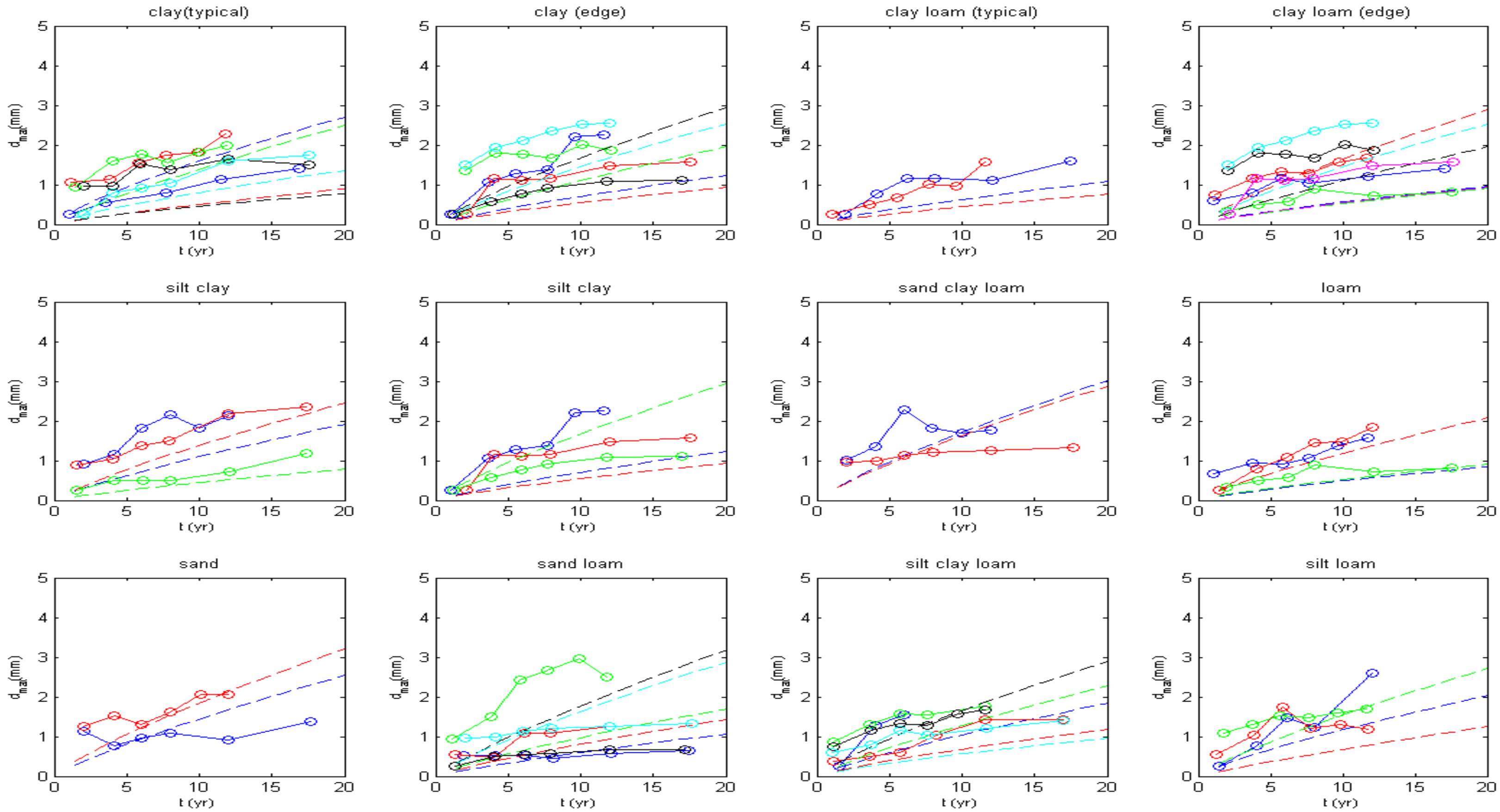

Figure 11. Plots of actual and predicted maximum pit depths vs. exposure time determined from the regression coefficients for sandy clay loam as determined by Caleyo.

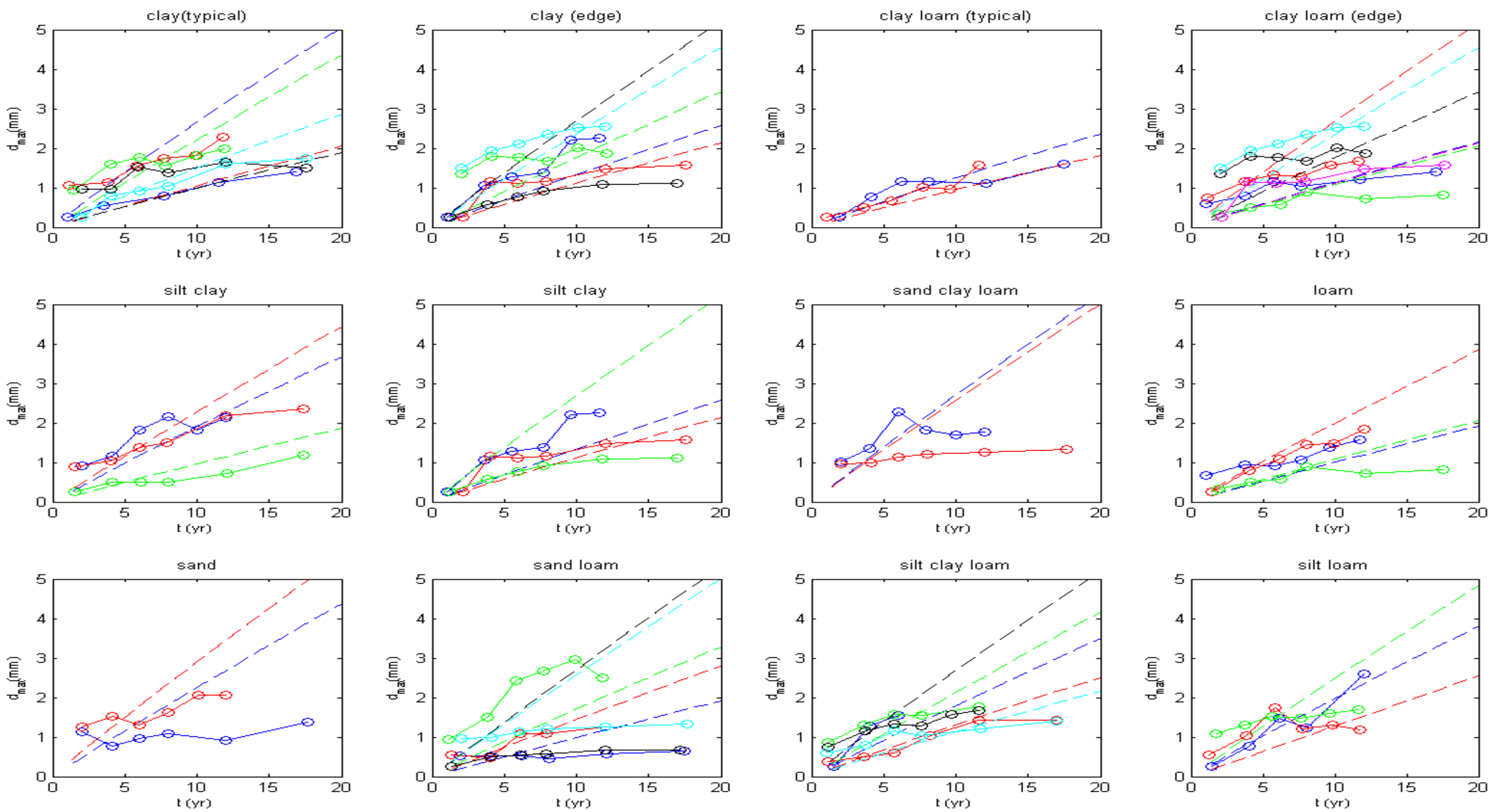

Figure 12. Plots of actual and predicted maximum pit depths vs. exposure time determined from the regression coefficients for "all" soil as determined by Caleyo.

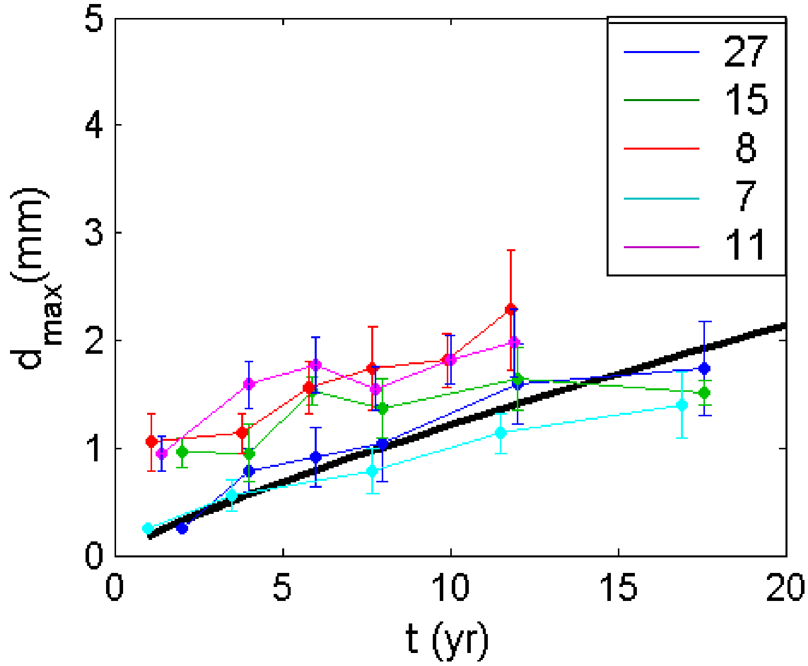

Figure 13. Plot of maximum pit depth versus exposure time for NIST clay site data compared to Caleyo published data for clay soil. The black line is the Caleyo data and the colored data are the NIST data sites.

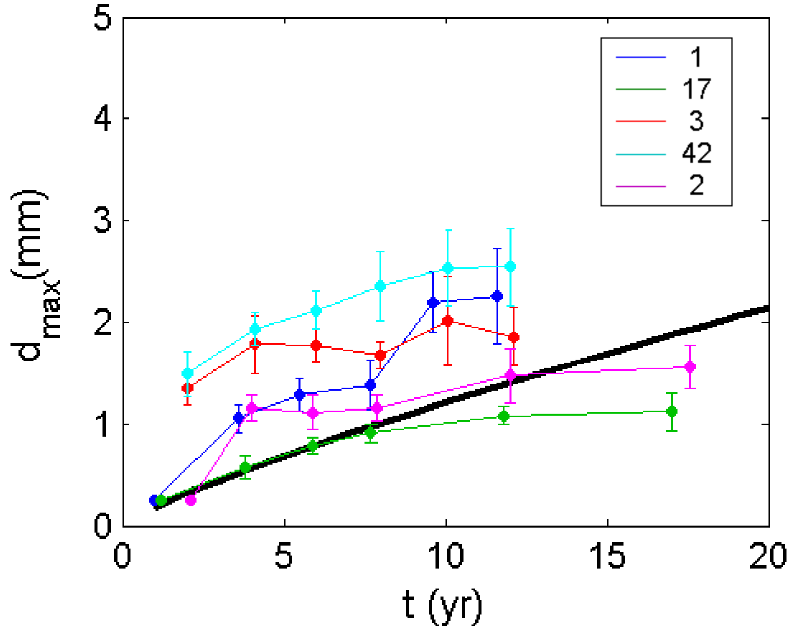

Figure 14. Plot of maximum pit depth versus exposure time for additional NIST clay site data compared to Caleyo published data for clay soil. The black line is the Caleyo data and the colored data are the NIST data sites.

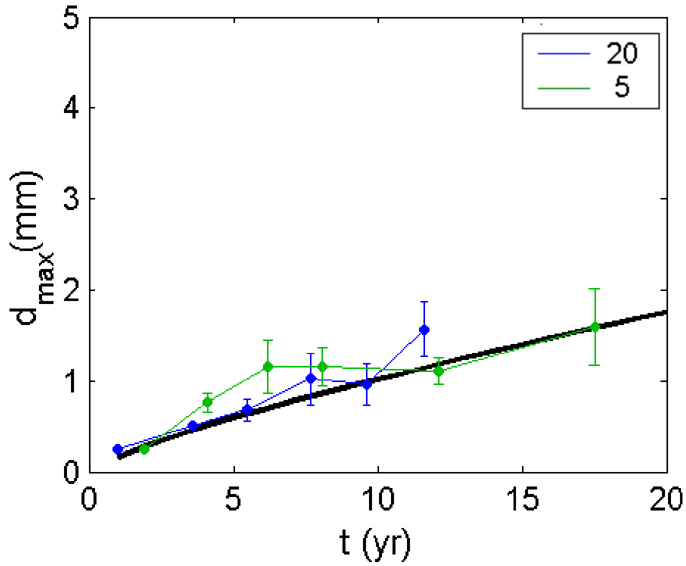

Figure 15. Plot of maximum pit depth versus exposure time for NIST clay loam site data compared to Caleyo published data for clay loam soil. The black line is the Caleyo data and the colored data are the NIST data sites.

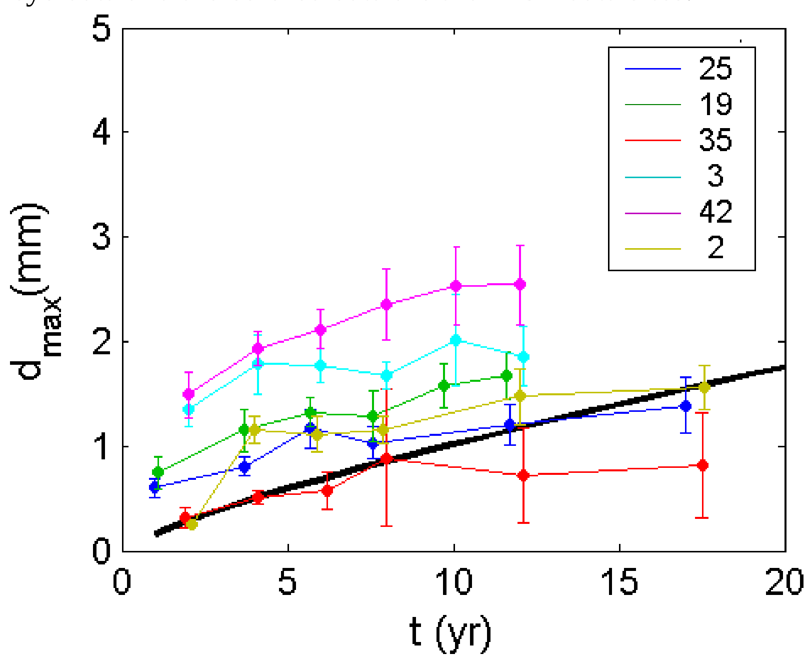

Figure 16. Plot of maximum pit depth versus exposure time for additional NIST clay loam site data compared to Caleyo published data for clay loam soil. The black line is the Caleyo data and the colored data are the NIST data sites.

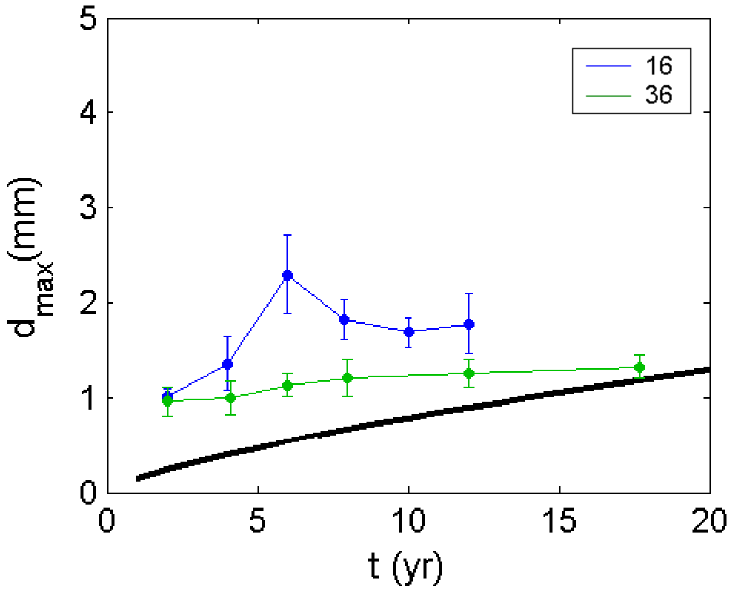

Figure 17. Plot of maximum pit depth versus exposure time for NIST sandy clay loam site data compared to Caleyo published data for sandy clay loam soil. The black line is the Caleyo data and the colored data are the NIST data sites.

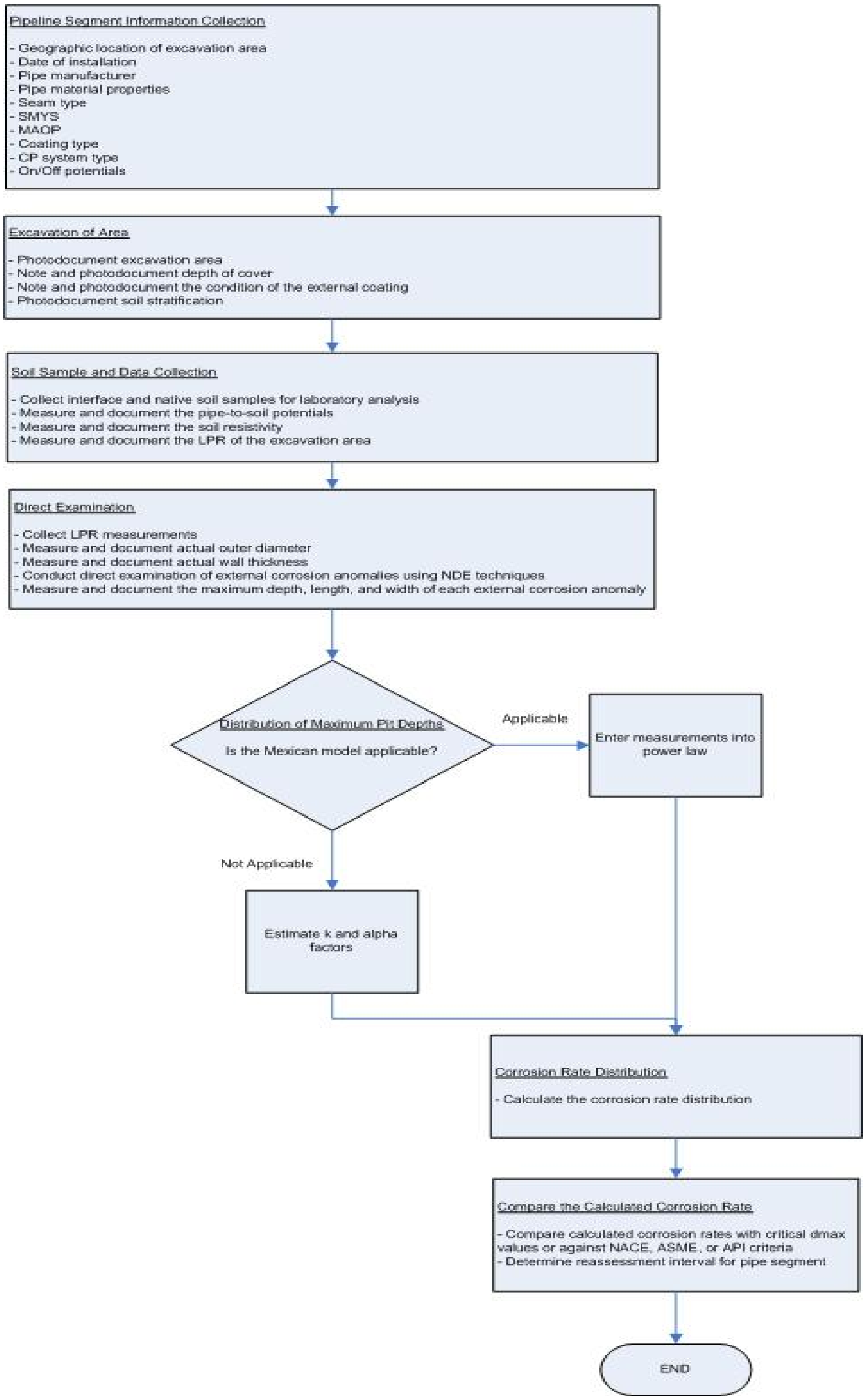

Figure 18. Flow diagram showing reassessment protocol.

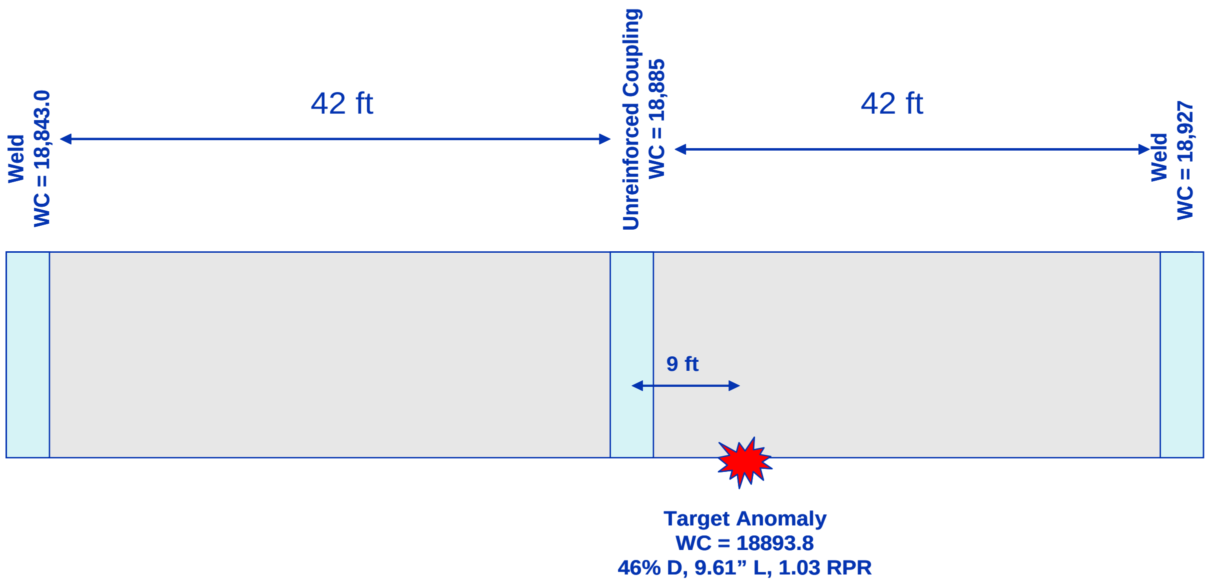

Figure 19. Schematic showing the location of the target anomaly from Site A2.

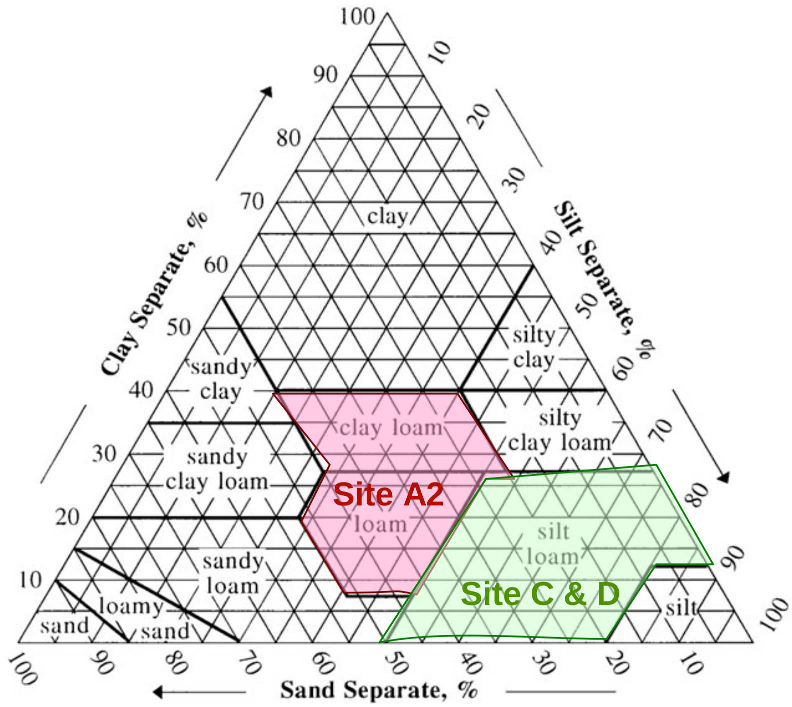

Figure 20. Soil classification plot showing the soil types determined for the field dig sites.

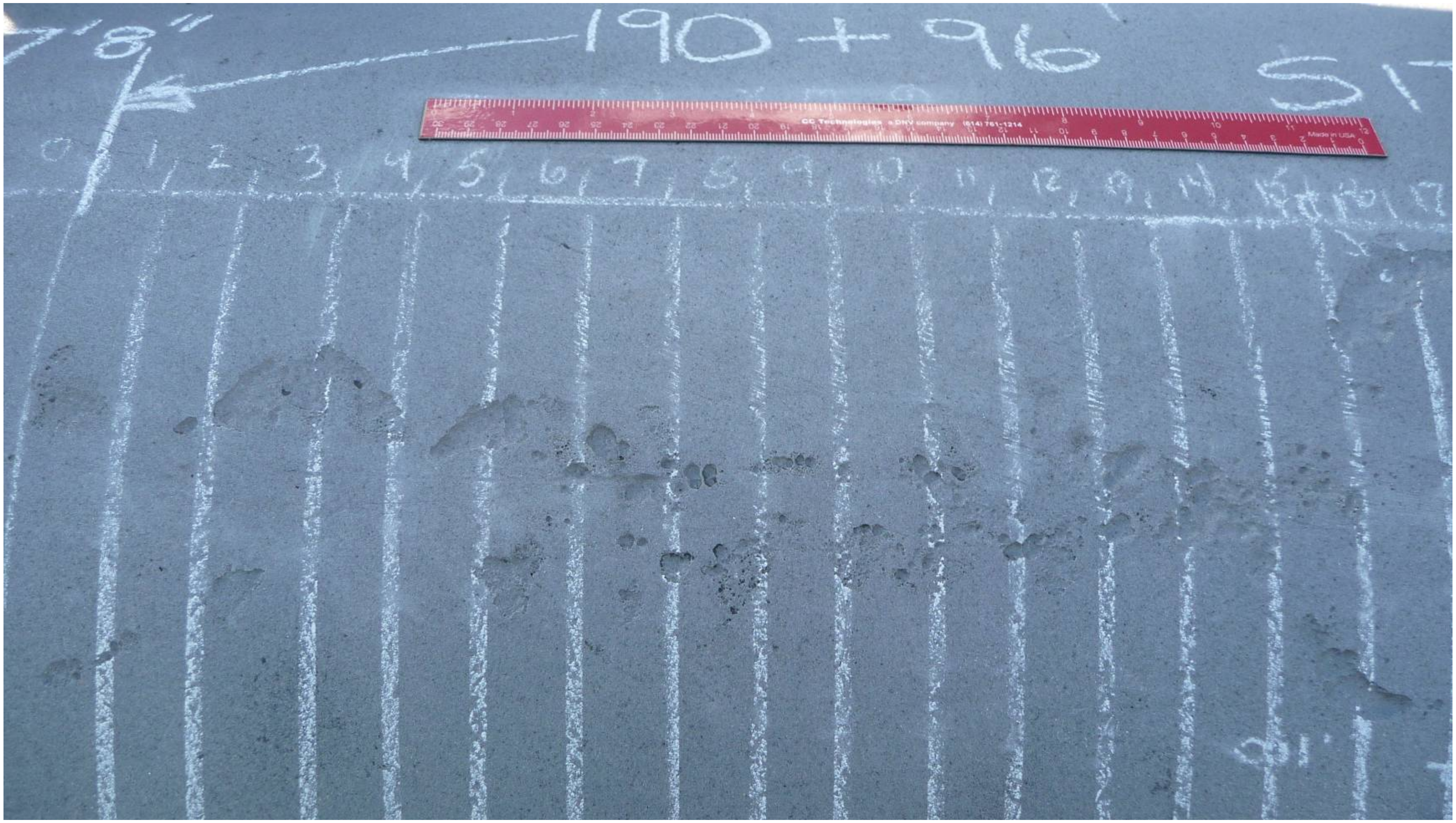

Figure 21. Photograph of the target anomaly area from Dig Site A2 after the pipe was sandblasted.

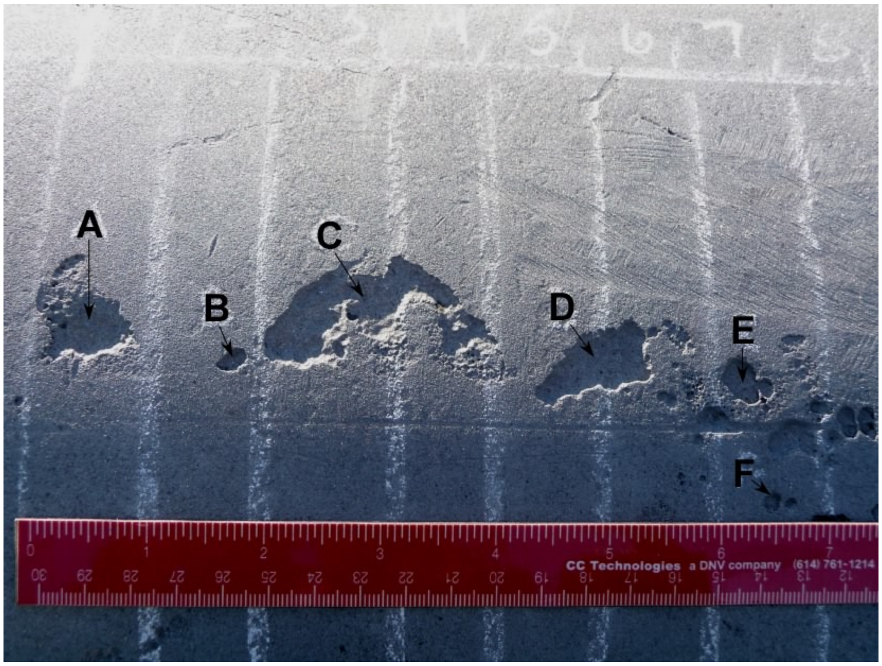

Figure 22. Photograph showing Pits A – F from Dig Site A2.

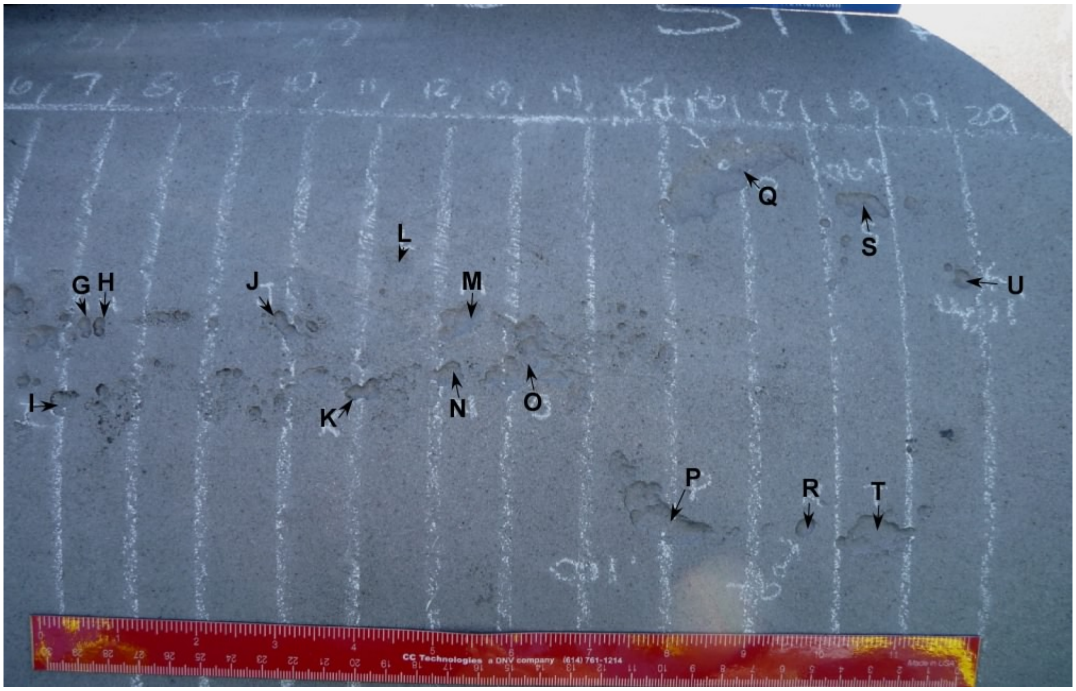

Figure 23. Photograph showing Pits G – U from Dig Site A2.

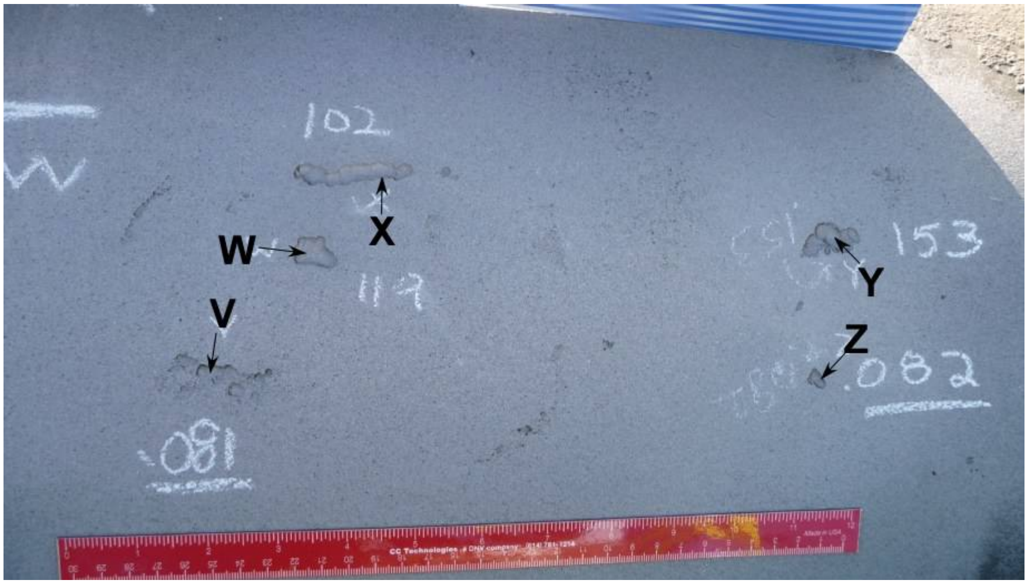

Figure 24. Photograph showing Pits V – Z from Dig Site A2.

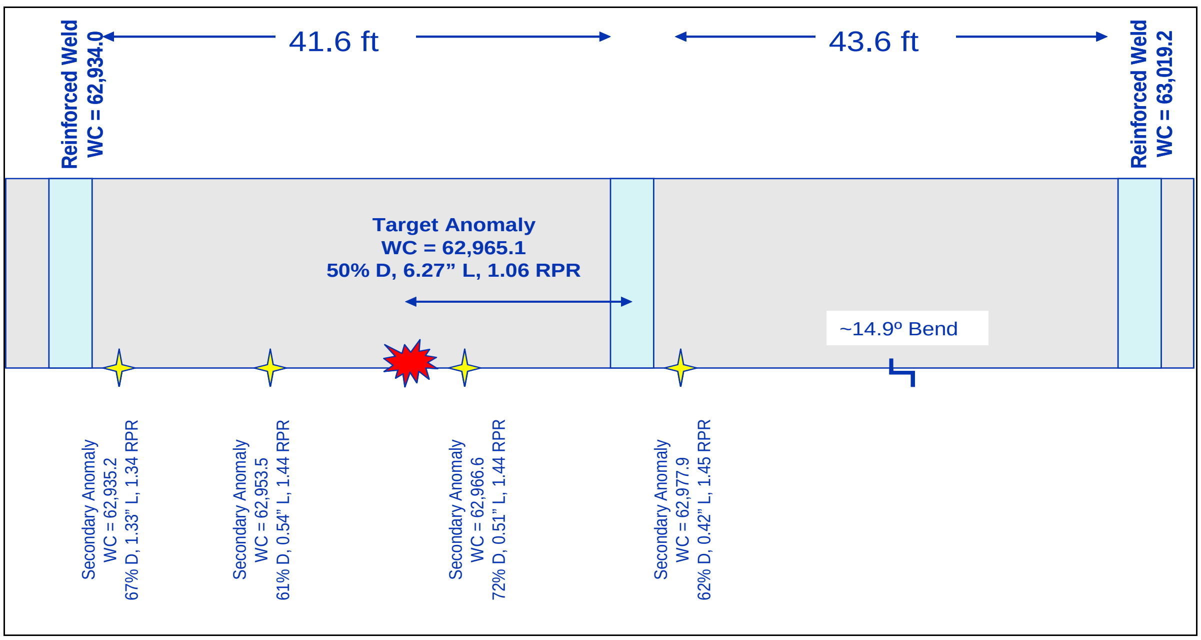

Figure 25. Schematic showing the location of the target anomaly from Site C.

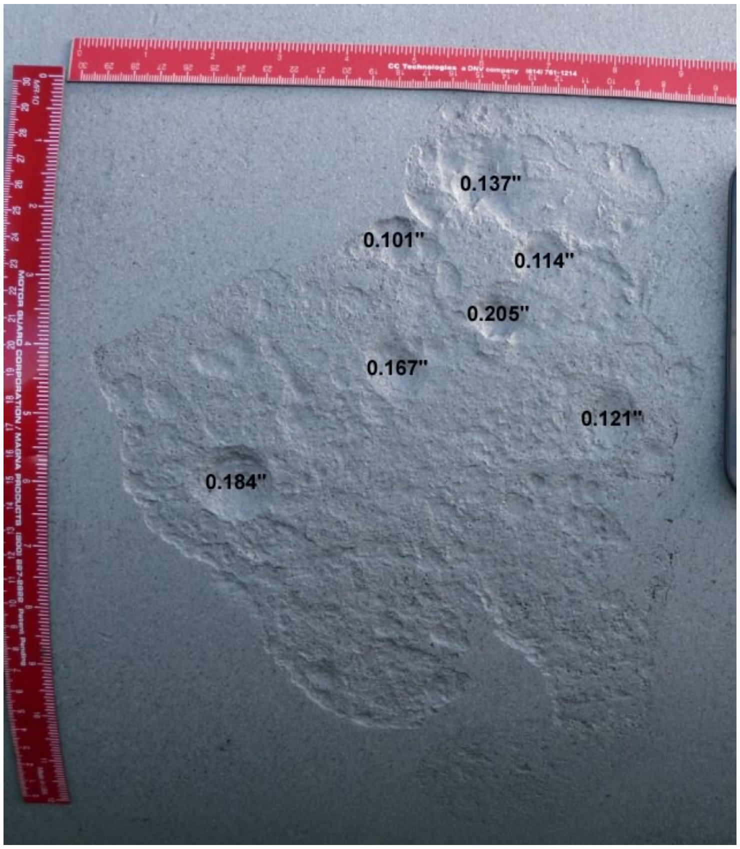

Figure 26. Photograph of target anomaly from Site C, after it was sandblasted. Pit depths are identified in black.

Figure 27. Photograph of Secondary Anomaly A from Site C.

Figure 28. Photograph of Secondary Anomaly B from Site C.

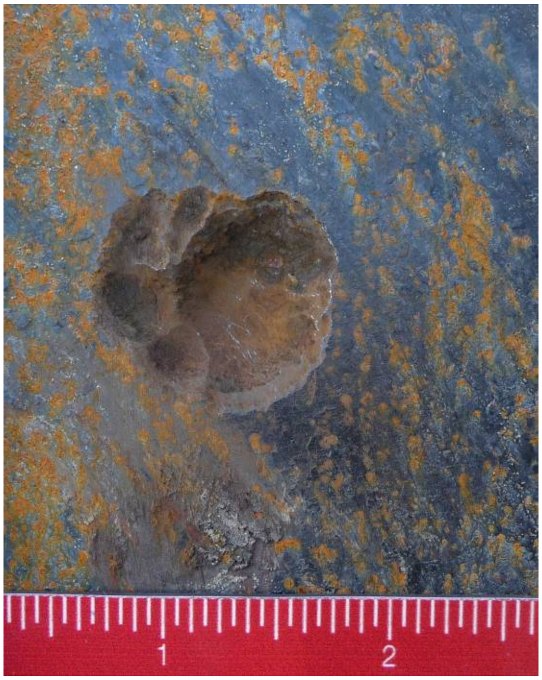

Figure 29. Photograph of Secondary Anomaly C from Site C.

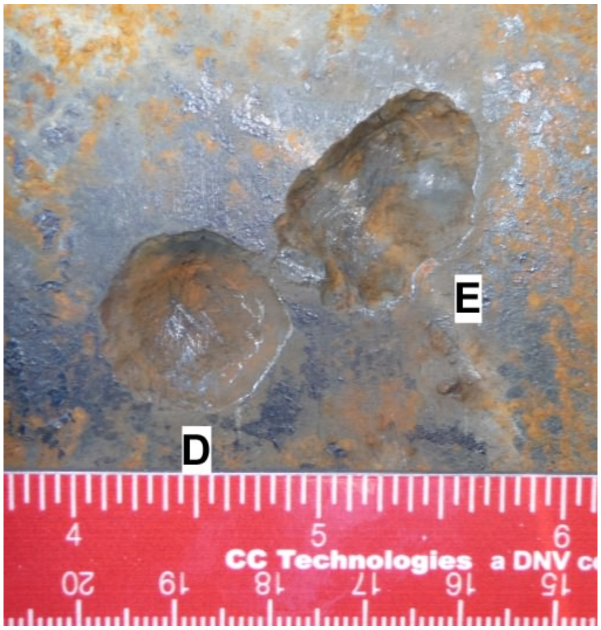

Figure 30. Photograph of Secondary Anomalies D and E from Site C.

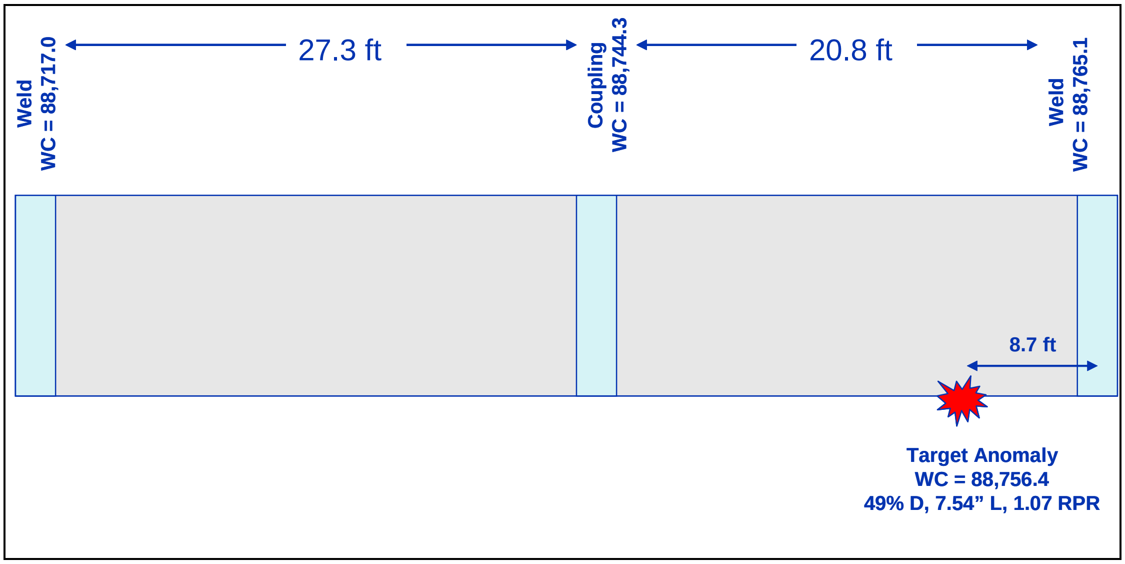

Figure 31. Schematic showing the location of the target anomaly from Site D.

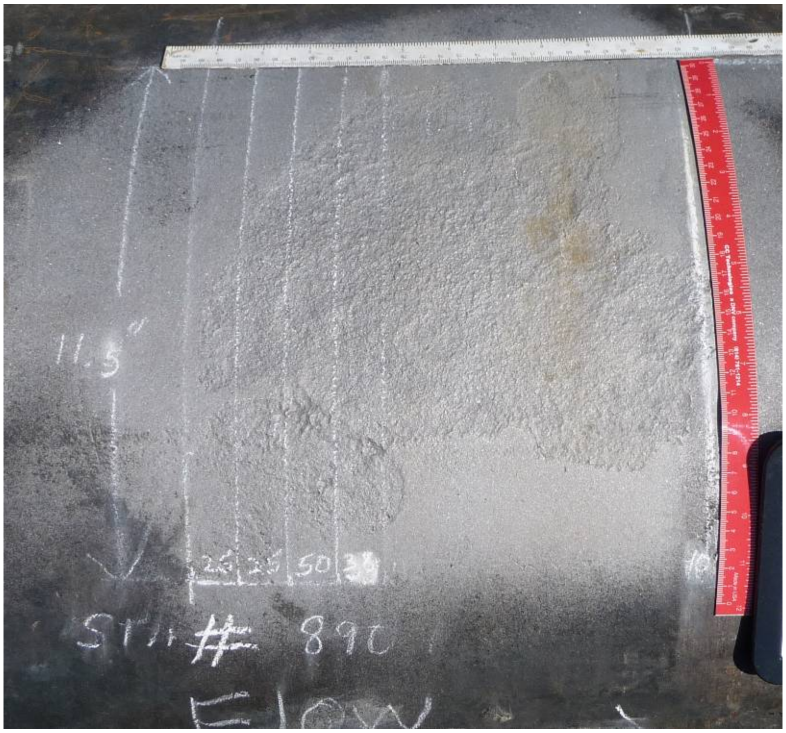

Figure 32. Photograph of the target anomaly at Dig Site D, after sandblasting.

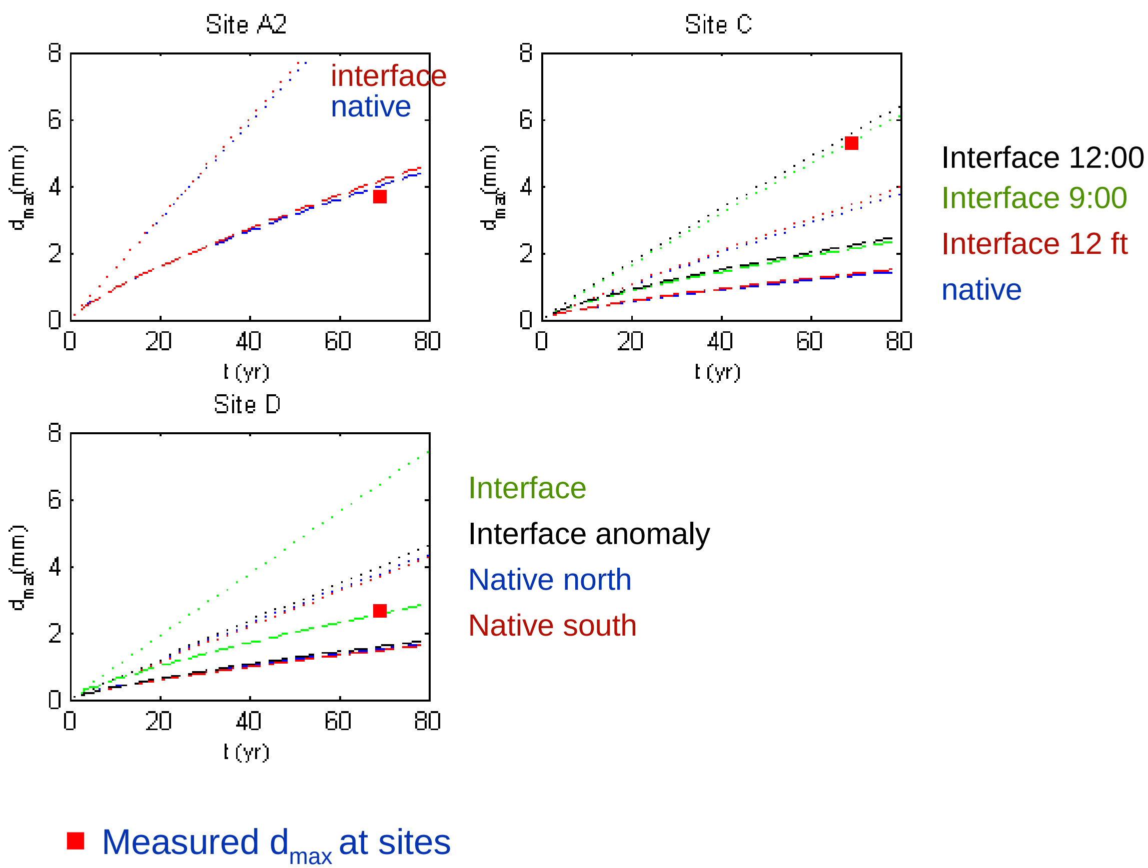

Figure 33. Plots of predicted maximum pit depth vs. exposure time for Dig Sites A2, C, and B using multiple soil data for each site and Caleyo's "Clay" Model. The dotted line data were predicted using an upper boundary value for the pipe to soil potential and the dashed line data were predicted using a mean value for the pipe to soil potential.

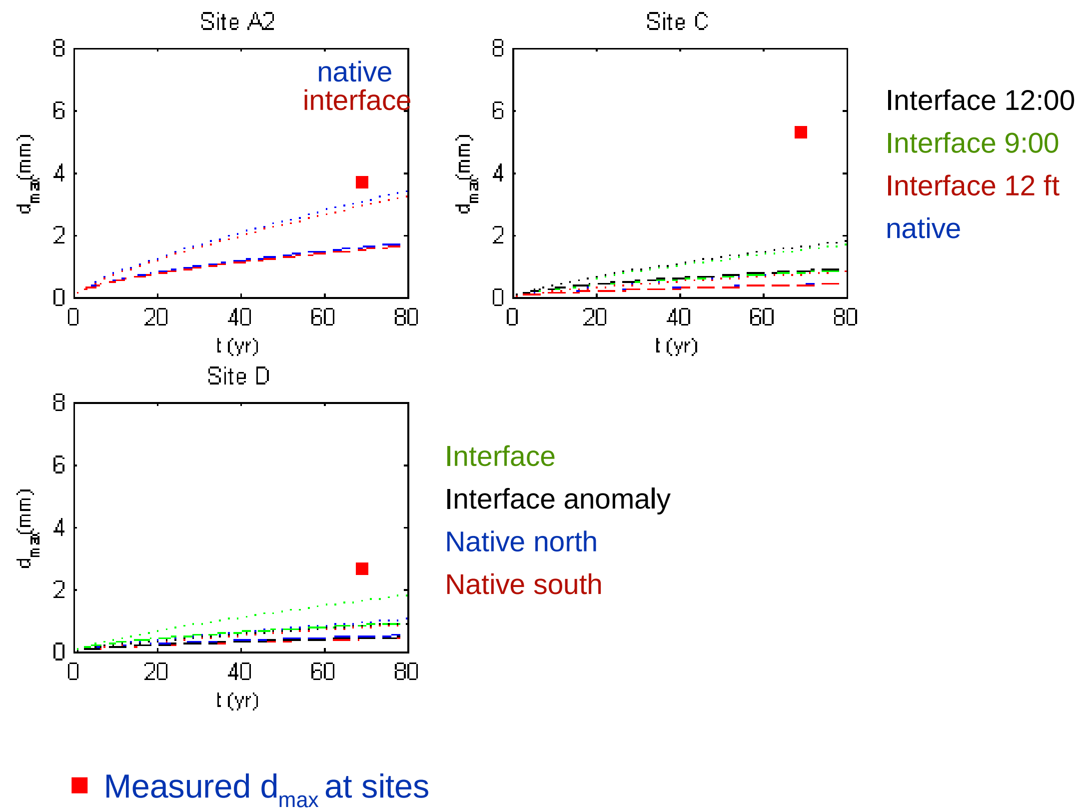

Figure 34. Plots of predicted maximum pit depth vs. exposure time for Dig Sites A2, C, and B using multiple soil data for each site and Caleyo's "Sandy Clay Loam" Model. The dotted line data were predicted using an upper boundary value for the pipe to soil potential and the dashed line data were predicted using a mean value for the pipe to soil potential.

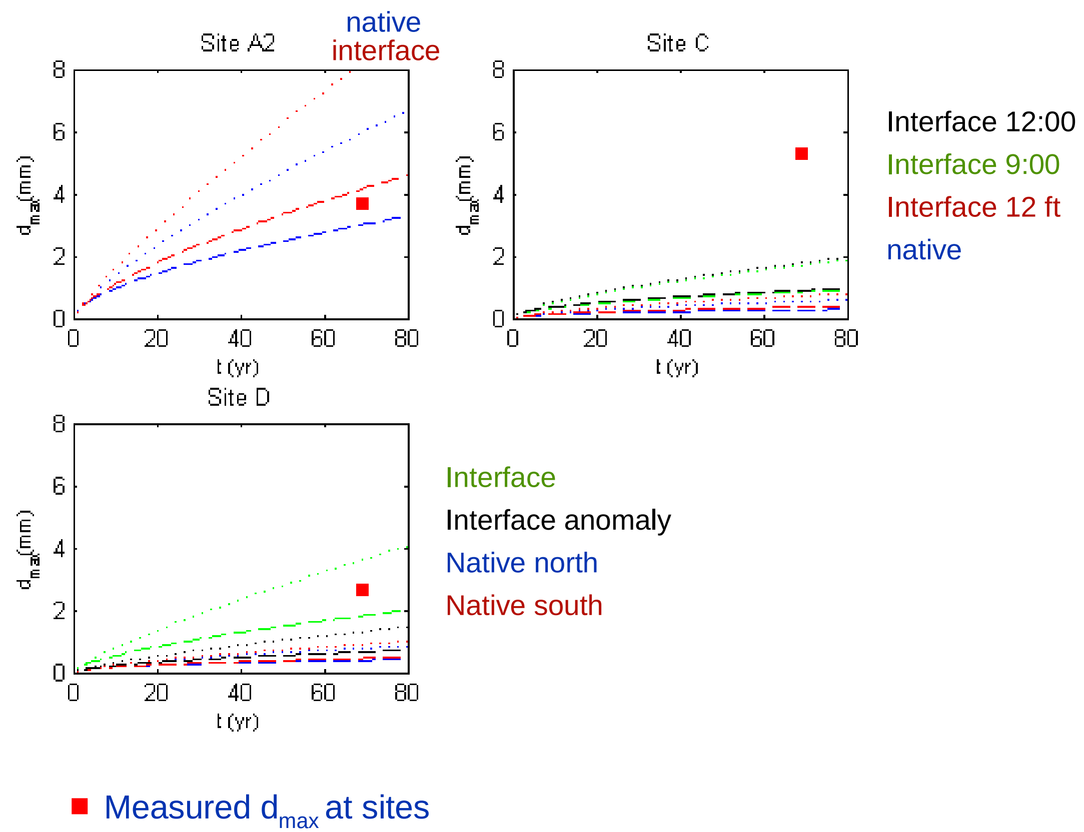

Figure 35. Plots of predicted maximum pit depth vs. exposure time for Dig Sites A2, C, and B using multiple soil data for each site and Caleyo's "Clay Loam" Model. The dotted line data were predicted using an upper boundary value for the pipe to soil potential and the dashed line data were predicted using a mean value for the pipe to soil potential.

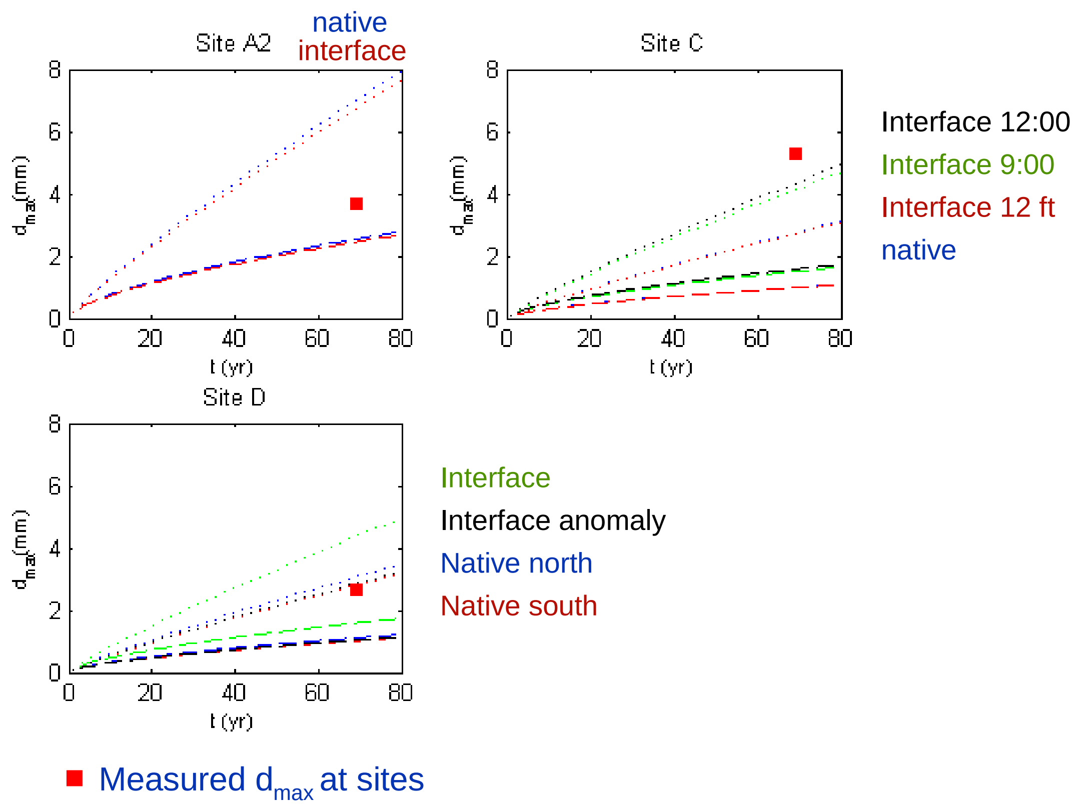

Figure 36. Plots of predicted maximum pit depth vs. exposure time for Dig Sites A2, C, and B using multiple soil data for each site and Caleyo's "All" soil Model. The dotted line data were predicted using an upper boundary value for the pipe to soil potential and the dashed line data were predicted using a mean value for the pipe to soil potential.

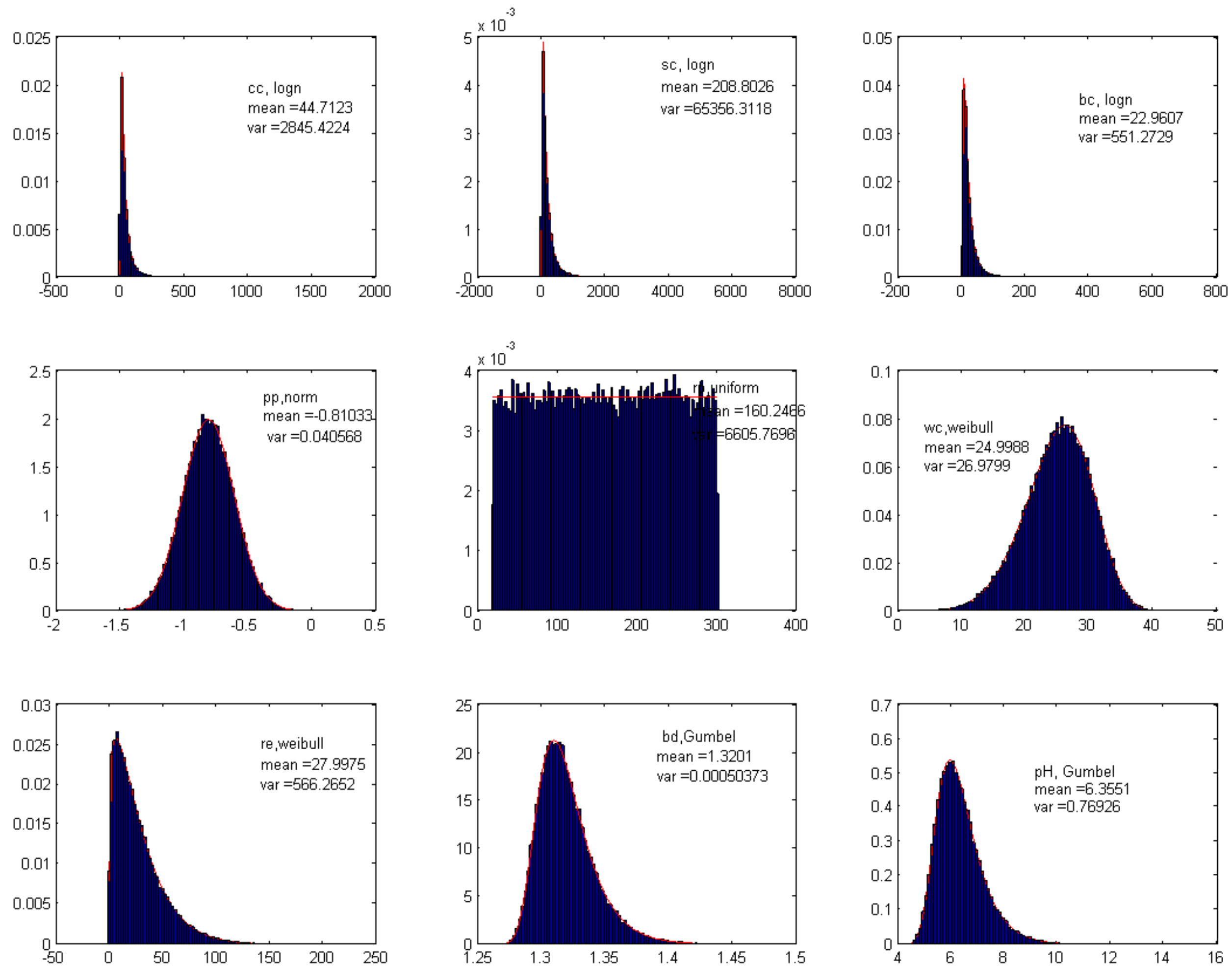

Figure 37. Plots of the generated parameter distributions for Dig Site A2 identified in Caleyo's modified power law model.

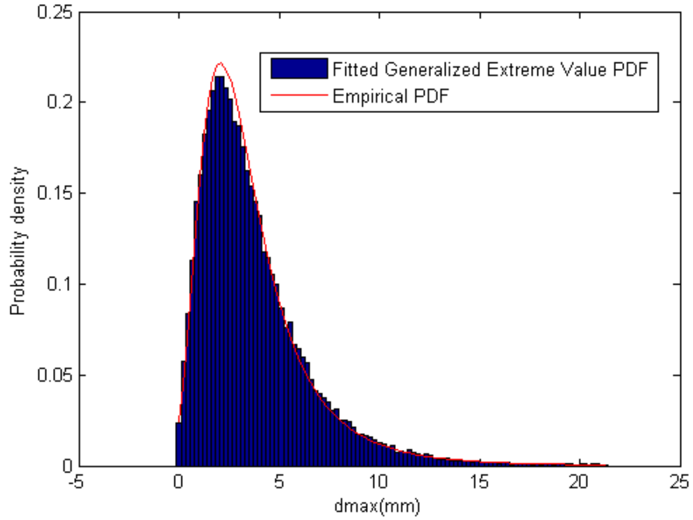

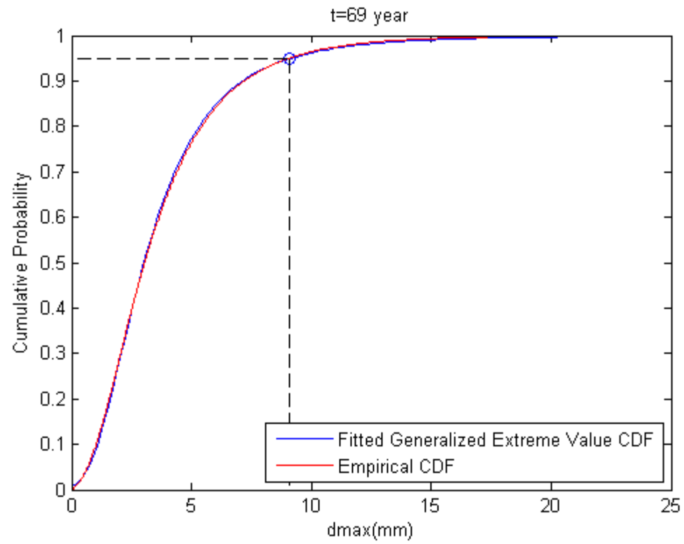

t (yr)	time interval (yr)	mean (dmax)	std(dmax)	CDF<=0.95
69	0	3.722	2.755	9.151
72	3	3.826	2.87	9.388
74	5	3.903	2.932	9.574
76	7	3.963	3	9.8
79	10	4.089	3.116	10.186

Figure 38. Maximum pit depth distribution calculated for Site A2 (exposure time = 69 years): probability distribution function (Top Left), cumulative distribution function (Top Right), and table of predicted maximum pit depths (Bottom).

DNV Energy

DNV Energy is a leading professional service provider in safeguarding and improving business performance, assisting energy companies along the entire value chain from concept selection through exploration, production, transportation, refining, and distribution. Our broad expertise covers Asset Risk & Operations Management, Enterprise Risk Management; IT Risk Management; Offshore Classification; Safety, Health and Environmental Risk Management; Technology Qualification; and Verification.

DNV Energy Regional Offices:

Asia and Middle East
Det Norske Veritas Sdn Bhd
24th Floor, Menara Weld
Jalan Raja Chulan
50200 Kuala Lumpur
Phone: +603 2050 2888

North America
Det Norske Veritas (USA), Inc.
1400 Ravello Drive
Katy, TX 77449
United States of America
Phone: +281-396-1000

Europe and North Africa
Det Norske Veritas Ltd
Palace House
3 Cathedral Street
London SE1 9DE
United Kingdom
Phone: +44 20 7357 6080

Offshore Class and Inspection
Det Norske Veritas AS
Veritasveien 1
N-1322 Hovik
Norway
Phone: +47 67 57 99 00

Cleaner Energy & Utilities
Det Norske Veritas AS
Veritasveien 1
N-1322 Hovik
Norway
Phone: +47 67 57 99 00

South America and West Africa
Det Norske Veritas Ltda
Rua Sete de Setembro
111/12 Floor
20050006 Rio de Janeiro Brazil
Phone: +55 21 2517 7232

Nordic and Eurasia
Det Norske Veritas AS
Veritasveien 1
N-1322 Hovik
Norway
Phone: +47 67 57 99 00